AIAA JOURNAL
Vol. 49, No. 5, May 2011

Residual Distribution Method for Aeroacoustics

L. Koloszár,* N. Villedieu,† T. Quintino,† P. Rambaud,‡ H. Deconinck,§ and J. Anthoine¶
von Kármán Institute for Fluid Dynamics, 1640 Rhode-St-Genèse, Belgium

DOI: 10.2514/1.J050645

This article deals with the discretization of linearized Euler equations by multidimensional upwind residual distribution methods. Linearized Euler equations are applied to model the propagation of sound in the domain where no source of sound is present and where the analogy methods such as Ffowcs–Williams can not be used because of gradients in the mean flow. The residual distribution method leads to a class of schemes that shares properties of both finite element method and finite volume method. In particular, the schemes used here are multidimensional upwind, which make them very attractive because of their low cross-dissipation. First, the discretization method is introduced as an alternative method for computational aeroacoustic applications on unstructured grids. The residual distribution method is then analyzed analytically for wave propagation. Next it is applied to linearized Euler equations with proper acoustic boundary conditions, and finally verifiedon test cases having exact solution.

Nomenclature

A, B	=	system Jacobian matrices
B	=	system distribution matrix
C_i	=	scaling of the pseudotime
c	=	speed of sound
$\mathbf{F}$, $\mathbf{G}$	=	fluxes
$\mathbf{H}$	=	term due to the nonuniform mean flow
H	=	(time dependent) 1-D linear basis function
K	=	system upwind matrix
M	=	Mach number
$\mathbf{n}$	=	inward normal vector
$\mathbf{n}$	=	inward normal vector
p	=	pressure
S_T	=	median area of the triangle T
$\mathbf{U}$	=	vector of conserved quantities
$\mathbf{U}$	=	vector of conserved quantities
u	=	scalar variable
u^h	=	numerical approximation of the scalar variable
u_j	=	velocity component in the j direction
β	=	distribution coefficient
κ	=	scalar upwind coefficient
$\boldsymbol{\lambda}$	=	convection vector
ρ	=	density
τ	=	pseudotime
Φ	=	residual
ψ	=	(space-dependent) linear continuous Lagrangian basis function
Ω	=	numerical domain
$()'$	=	small perturbation quantities
$()_0$	=	mean flow quantities

Introduction

SOUND production and propagation is an unsteady process. Sound waves propagate coherently over long distances with very low attenuation due to viscous effects. On the other hand, even a very loud flow radiates only a small fraction of its total energy as sound which means that the perturbations to the mean flow are very small. Therefore, the numerical resolution to capture the sound propagation has to be very high [1]. Various methods have been applied successfully to propagate noise in homogeneous and inhomogeneous background flows [2], however, the tradeoff between accuracy and computational cost still leaves room for further investigations on more efficient and robust solvers. A possible approach to encounter these requirements is to treat separately noise production from noise propagation. The propagation part of such a hybrid method is considered in this paper.

A balance between resolution, accuracy, and computing time requirements always has to be kept when numerical simulations are considered. Except for academic problems direct numerical simulation and even the less expensive large eddy simulation are unaffordable for unsteady flow calculations in large fields such as the ones involved for sound propagation. In the region where no more sound production occurs, but mean flow gradients are still present, the Linearized Euler Equations (LEEs) fully describe the wave propagation including reflection, scattering and refraction effects. Further, where the background flow can be considered as uniform, computationally less expensive integral methods such as Curle's analogy or Ffowcs–Williams and Hawkings equation can be used.

The requirements on the numerical schemes in case of discretization of sound propagation are rather restrictive. To propagate waves over long distances with negligible dissipation and without phase error, a consistent, stable, and convergent high-order scheme is not enough to guarantee a good quality for the numerical wave solution [3]. Indeed, wave propagation involves the interplay between space and time. So, to be able to compute a wave solution accurately it is not sufficient to have a good approximation of the spatial derivatives alone or of the time derivatives alone. Both of them must be well approximated in a related way as dictated by the dispersion relation of the original partial differential equation, otherwise the wave modes may become numerically coupled. To get the same accuracy and dispersion/dissipation relation in space and time a coupled space-time discretization method is used in this paper.

Several ways have been proposed to discretize wave propagation equations. The spectral difference method is very efficient for simple geometries and boundary conditions. These methods have no dispersion error, but are only applicable for uniform grids. Finite difference methods are commonly used when the LEEs are under consideration. High-order schemes can be implemented in a rather straightforward way and even special optimized schemes [4] are available for acoustic propagation problems (the effective wave number of the scheme is close to the actual one for frequencies as high as possible). The main disadvantage is that it can be used with full effectiveness only in case of structured quadrilateral grids. From the family of finite element methods, mainly the discontinuous

Presented as Paper 2009-3116 at the 15th AIAA/CEAS Aeroacoustics Conference, Miami, FL, 11–13 May 2009; received 22 June 2010; revision received 6 December 2010; accepted for publication 10 December 2010.

*Member of Doctoral Programme; koloszar@vki.ac.be.
†Senior Research Engineer.
‡Assistant Professor.
§Professor.
¶Associate Professor.

Galerkin method is used to calculate wave propagation [5]. Its advantage is the easy implementation of high-order polynomial basis functions. However, the upwinding of interelement fluxes introduces numerical dissipation. The effect of numerical dissipation can be diminished with increasing polynomial order. Its main advantage over all the other methods is that it can be applied over complex unstructured grids and the communication between the elements through fluxes makes the parallelization straightforward. On the other hand the discontinuous representation of variables results in N times higher degrees of freedom than in case of continuous representation, where N is the number of nodes per element (in case the nodes are on the faces). An alternative approach followed in this paper is the residual distribution method (RDM), described in detail below.

RDM

The residual distribution or fluctuation splitting method is somewhere between the finite element and finite volume methods. The idea was introduced in 1982 by Roe [6] and extended in 1986 for the solution of conservation laws on unstructured meshes. In the last decades several multidimensional upwind schemes have been developed [7,8] and proved to be accurate and robust. A new strategy in the computation of the residuals have been designed involving contour integrations and leading to conservative discretization even for problems where it is not possible to linearize the system of equations [9]. Thanks to this improvement the application of residual distributive schemes (RDS) to high-order discretization was possible. Abgrall [10] and Tave et al. [11] developed the Lax–Friedrichs scheme that uses a central distribution of the residual which makes the distribution in high-order elements easy and efficient. In our case, since we want to distribute to the downwind nodes it is necessary to split the high-order elements in linear elements where we know how to use a multidimensional upwind distribution [10,12]. Several methods has been developed to solve unsteady problems [13–16]. In this work we decided to focus on two of them, representing the two major types of time discretization in RDS. The first one was developed by Abgrall and Mezine [13] and uses a finite elementlike approach with a mass matrix. The second method considers the time as a third dimension yielding space-time element and was first presented by Ricchiuto [17]. In this article we will apply the above-mentioned methods to acoustic problems which is a new application of RDS.

The higher accuracy and compact character make the RDS very efficient. The main advantage of the method is that both oscillation free and higher-order approximation can be achieved on unstructured grid based on the compact stencil of the nearest neighborhood, which leads to easy parallel implementation. From mathematical point of view the RD method is a continuous approximation of the variables and the multidimensional upwinding minimizes the amount of crosswind diffusion. The aim of this paper is to show that, thanks to the properties mentioned above, RDS can be an alternative to discontinuous Galerkin and finite difference for wave propagation problems. In particular, we will show that the results obtained are comparable to high-order finite difference results. In this section, for simplicity, we first present the RD method for a steady system of conservation laws. Next, we focus on the strategies used for unsteady problems and more particularly to the space-time formulation. Then the high-order discretization is derived and finally the extension to system of equations is shown.

Steady Scalar Advection

To show the method of discretization, we first consider a steady scalar conservation law:

$$\nabla \cdot \mathcal{F}(u) = S \quad \forall\ (x, y) \in \Omega \Longleftrightarrow \left(a\frac{\partial u}{\partial x} + b\frac{\partial u}{\partial y} = S \right) \tag{1}$$

For a given domain Ω let denote by τ_h a generic triangulation of Ω composed of a set of nonoverlapping triangles $T \in \tau_h$ (Fig. 1).

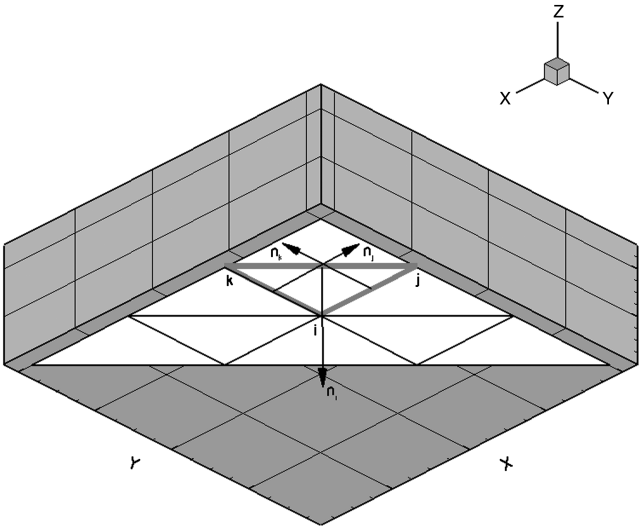

Fig. 1 Generic nonoverlapping triangulation.

Following the finite element way to discretize, for any given function u we define the approximate solution:

$$u^h = \sum_{i \in \tau_h} \psi_i u_i \tag{2}$$

where u_i is the value of u^h at node i: $u_i = u^h(x_i, y_i)$; and $\psi_i(x, y)$ denotes the (mesh dependent) linear continuous Lagrangian basis function. An example of such an approximation is illustrated in Fig. 2.

To solve Eq. (1), we compute the residual due to the discretization on each element T:

$$\Phi^T = \Phi^{\text{adv}} + \Phi^s = \int_T \nabla \mathcal{F}^h \, \mathrm{d}\Omega - \int_T S^h(x, y) \, \mathrm{d}\Omega \tag{3}$$

The residual Φ^{adv} can be computed either by integrating directly on the element or with the help of Gauss theorem by computing the contour integral. The later developed by Ricchiuto et al. [9] and Ricchiuto [17] is called conservative residual distribution (CRD) because this formulation ensures conservation. In this work we only consider CRD schemes. If we use a contour integration, then the residual is:

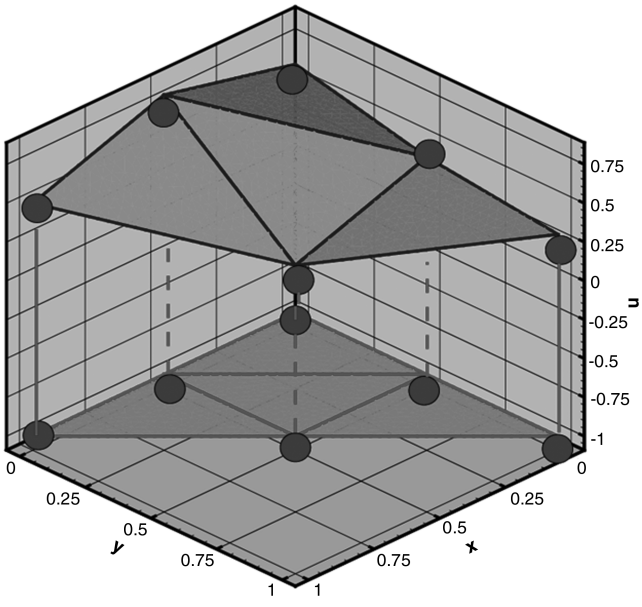

Fig. 2 Approximation of u by a linear approximation.

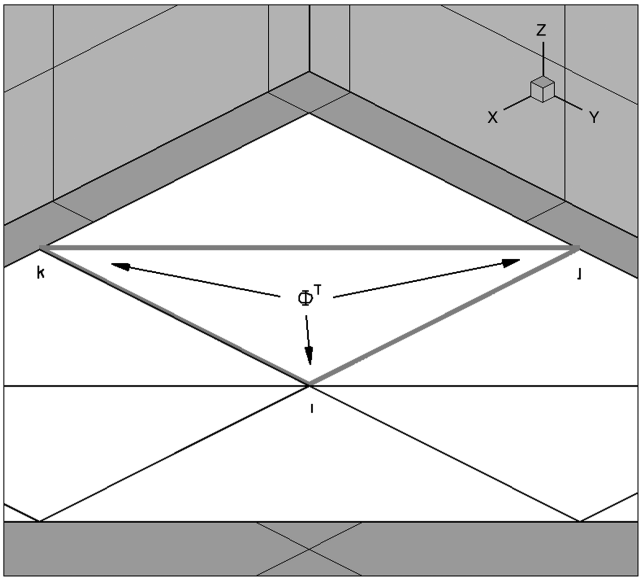

Fig. 3 Distribution of the global residual from element T to nodes i, j, k.

$$\Phi^{\text{adv}} = \oint_{\partial T} \mathcal{F}^h \cdot \mathrm{d}\boldsymbol{l} \tag{4}$$

The next step is the distribution of the residual Φ^T (see Fig. 3) to each node of T. This is done by means of a distribution coefficient β_i^T. With the distribution we obtain a part of the nodal residual (belonging to node i):

$$\Phi_i^T = \beta_i^T \Phi^T \tag{5}$$

To ensure consistency it is necessary that

$$\sum_{i\in T} \beta_i^T = 1 \Longleftrightarrow \sum_{i\in T} \Phi_i^T = \Phi^T \tag{6}$$

The different choices of β_i define the different numerical schemes with their own characteristics. It is possible to construct multidimensional upwind schemes which gives the major difference to other methods like finite difference (FD), finite volume (FV), or the classical finite element (FE). In the case of multidimensional upwinding the residual is only distributed to nodes which are downstream with respect to the orientation of the convection direction $\boldsymbol{\lambda} = (a, b)$. We can define for each node in each triangle an upwind parameter as:

$$\kappa_i = \frac{1}{2}\boldsymbol{\lambda} \cdot \mathbf{n}_i \tag{7}$$

where $\mathbf{n}_i$ is the inward normal to the edge of T facing node $i \in T$, while $|T|$ is the area of the triangle T. The norm of $\mathbf{n}_i$ is equal to the length of the edge (Fig. 1).

Then, an upwind scheme is a scheme such that:

$$\kappa_i < 0 \Rightarrow \beta_i = 0 \tag{8}$$

Remark: *This upwind parameters are also used to compute the residual when integration on linear elements are considered to get the residual:*

$$\Phi^T = \sum_{i\in T} \kappa_i u_i \tag{9}$$

The scheme used in the present work is called Low Diffusion A (LDA) because it is one of the least dissipative schemes. For this reason it is well fit for acoustic problems. Indeed, if we consider the scalar advection on a mesh aligned with the advection direction, the inlet is exactly preserved. The distribution coefficient of LDA is defined by:

$$\beta_i^{\text{LDA}} = \kappa_i^+ \left(\sum_{j\in T} \kappa_j^+ \right)^{-1} \tag{10}$$

where $\kappa_i^+ = \max(0, \kappa_i)$. This scheme is second-order accurate in case of linear elements (despite the fact that the stencil only involves the neighboring nodes) and third-order for quadratic ones.

Once the residual over each element is distributed to the nodes, all the contributions related to a node can be assembled (see Fig. 4). Finally, we solve the following system of nodal equations (the summation is done over the elements containing node i):

$$\sum_{T, i\in T} \Phi_i^T = 0 \qquad i = 1, \cdots, N \tag{11}$$

This system is solved by pseudotime iterations:

$$\frac{\partial u^h}{\partial \tau} + \sum_{T, i\in T} \Phi_i^T = 0 \tag{12}$$

For example, we can solve Eq. (12) by an explicit procedure like Forward–Euler method:

$$u_i^{\tau+1} = u_i^\tau - \frac{\Delta\tau}{C_i} \left(\sum_{T, i\in T} \Phi_i^T \right)^\tau \tag{13}$$

where C_i represents a scaling of the pseudotime, such that a CFL condition is verified. It is also possible to solve Eq. (12) using an implicit solver:

$$\frac{u_i^{\tau+1} - u_i^\tau}{\Delta\tau} = -\left(\sum_{T, i\in T} \Phi_i^T \right)^{\tau+1} \tag{14}$$

For more details on the linear solver we refer to the work of van der Weide [18].

Unsteady Scalar Advection

The extension of the residual distribution method to time dependent problem is not straightforward. The main problem is that if we just combine the spatial RD discretization with a finite difference method for the time dependency, then, in general, the scheme is only first-order accurate because in this way the spatial and time integration is not consistent. There are several ways to overcome this. The first approach is to use a finite elementlike mass matrix. The other way is to treat in a consistent way both space and time, which can be achieved by involving the time dependency in the RD formulation resulting in a space-time connection.

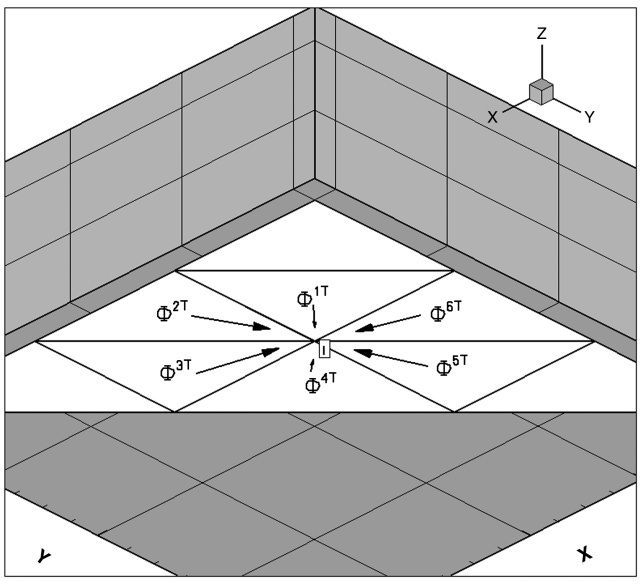

Fig. 4 Illustration of the system of Eq. (11).

Mass-Matrix Method: This method which has been first developped by Ferrante [19] and extended by Mezine et al. [13] uses an equivalence between Petrov-Galerkin (PG) and RD method to compute a mass matrix. The time dependency is discretized by a Crank-Nicolson method.

First, we want to link RD formulation with PG schemes. In this two methods the solution is discretized in the same way. Moreover, multidimensional upwinding RD methods are set for steady hyperbolic conservation law equations whereas PG can be used for any conservation law equations. Then, one idea to extend RD to more general set of equations is to use a Petrov-Galerkin approach. This is possible because we can find a weight function such that the two methodologies are equivalent in some cases.

Let consider the steady advection equation with a constant advection ($\boldsymbol{\lambda}$ is constant) and u^h is linear:

$$\boldsymbol{\lambda} \cdot \nabla u^h = 0 \tag{15}$$

We are looking for a weight function ω_i such that the contributions of the element T to the node i are the same for PG and RD method:

$$\beta_i^T \int_T \boldsymbol{\lambda} \cdot \nabla u^h \, \mathrm{d}\Omega = \int_T \omega_i \boldsymbol{\lambda} \cdot \nabla u^h \, \mathrm{d}\Omega$$

$$\beta_i^T |T| \boldsymbol{\lambda} \cdot \nabla u^h = \boldsymbol{\lambda} \cdot \nabla u^h \int_T \omega_i \, \mathrm{d}\Omega$$

This yields the following condition:

$$\int_T \omega_i \, \mathrm{d}\Omega = \beta_i^T |T| \tag{16}$$

Several weight functions verify this condition. We choose to use ω_i defined by:

$$\omega_i(x, y) = \psi_i(x, y) + \left(\beta_i^T - \frac{1}{3}\right)\chi^T(x, y) \tag{17}$$

where χ^T is the characteristic function of the element T:

$$\chi^T(x, y) = \begin{cases} 1 & \text{if } (x, y) \in T \\ 0 & \text{if } (x, y) \notin T \end{cases} \tag{18}$$

Let consider the unsteady advection equation:

$$\frac{\partial u}{\partial t} + \nabla \boldsymbol{\mathcal{F}} = S \quad \forall \ (x, y, t) \in \Omega_t = \Omega \times [0, t_f] \tag{19}$$

First, we apply the equivalence of last paragraph to our problem.

$$\Phi_i^T = \underbrace{\int_T \omega_i \sum_{j \in T} \psi_j \frac{\partial u_j}{\partial t} \, \mathrm{d}\Omega}_{\mathrm{I}} + \underbrace{\int_T \omega_i \nabla \boldsymbol{\mathcal{F}} \, \mathrm{d}\Omega}_{\mathrm{II}} \tag{20}$$

The second part of this is equivalent to the residual of RD method for a steady problem. The first integral can be transformed as:

$$I = \sum_{j \in T} m_{ij} \frac{\partial u_j}{\partial t}, \qquad m_{ij} = \int_T \omega_i \psi_j \, \mathrm{d}\Omega \tag{21}$$

Assembling these two contributions we obtain:

$$\Phi_i^T = \sum_{j \in T} m_{ij} \frac{\partial u_j}{\partial t} + (\Phi_i^{T,\mathrm{adv}})^t \tag{22}$$

In this formulation a discretization of the time dependency is still missing. This can be done by a Crank-Nicolson method for example. The final residual is then:

$$\Phi_i^T = \sum_{j \in T} m_{ij}(u_i^{n+1} - u_i^n) + \frac{\Delta t}{2}((\Phi_i^{T,\mathrm{adv}})^{n+1} + (\Phi_i^{T,\mathrm{adv}})^n) \tag{23}$$

At each time iteration u_i^n is known and we want to compute u_i^{n+1}. We compute it explicitly by pseudotime iterations:

$$u_i^{n+1,\tau+1} = u_i^{n+1,\tau} + \frac{\Delta \tau}{C_i}\left(\sum_{T, i \in T} \Phi_i^T\right)^\tau \tag{24}$$

Space-time method [13,20] In this case, time is treated as another spacelike dimension and a consistent discretization is applied for the extended system using space-time elements (see Fig. 5). The basic consequence of the space-time discretization is that whatever the order of the space discretization it is inherited to the time discretization as well.

The space-time formulation is described through the unsteady scalar advection problem [Eq. (19)]. Since time is considered as a third dimension, Ω_t is discretized by a succession of prismatic elements as shown on Fig. 5. For any given function u, its restriction on the prism is defined by:

$$u^h(x, y, t) = \sum_l H^l(t) \sum_{i \in T} \psi_i(x, y) u_i^l \tag{25}$$

where u_i^l is the value of u^h at node i and time t_l: $u_i^l = u^h(x_i, y_i, t_l)$, H^l is the (time dependent) 1-D linear basis function and $\psi_i(x, y)$ denotes the (mesh dependent) linear continuous Lagrangian basis function. In each space-time element u^n is considered as known and u^{n+1} is the unknown. The process is exactly the same as for steady problems. The first step of the discretization is again the computation of the residual, now, on each space-time prism:

$$\Phi^K = \int_{t_n}^{t_{n+1}} \int_T \left(\frac{\partial u^h}{\partial t} + \nabla \cdot \boldsymbol{\mathcal{F}}^h\right) \mathrm{d}\Omega \, \mathrm{d}t \tag{26}$$

which after some algebra yields:

$$\Phi^K = \frac{|T|}{3} \sum_{i \in T} (u_i^{n+1} - u_i^n) + \frac{\Delta t}{2}((\Phi^T)^n + (\Phi^T)^{n+1})$$

The residual Φ^T—using the CRD method—is defined by Eqs. (4) and (3). The total residual Φ^K is distributed to the nodes of the prism. To respect the physical meaning of time, we do not want to distribute to the nodes of the level n. To do this, like in the steady case, space-time upwind parameters have been constructed using the space-time normals, giving for level n and $n + 1$:

$$\tilde{\kappa}_i^n = \frac{\Delta t}{2}\kappa_i - \frac{|T|}{3} \qquad \tilde{\kappa}_i^{n+1} = \frac{\Delta t}{2}\kappa_i + \frac{|T|}{3} \tag{27}$$

where $\Delta t = t^{n+1} - t^n$ and κ_i [Eq. (7)] is the upwind parameter of the steady scheme. These upwind parameters are used to define the space-time multidimensional upwinding:

$$\tilde{\kappa}_i^n < 0 \Rightarrow \Phi_i^n = 0 \qquad \tilde{\kappa}_i^{n+1} < 0 \Rightarrow \Phi_i^{n+1} = 0 \tag{28}$$

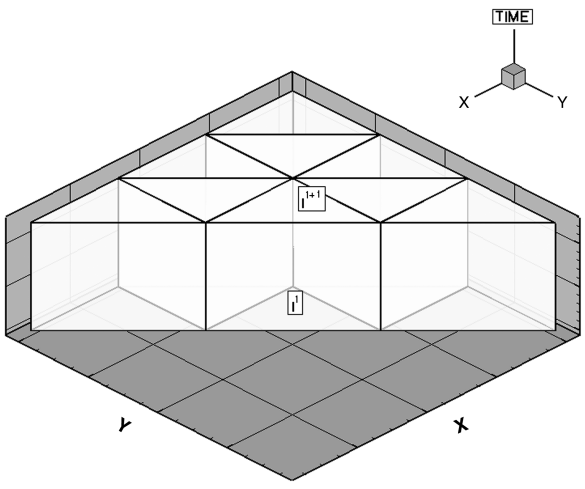

Fig. 5 Space-time prism.

Then, to be able to distribute the residual only to level $n+1$ we need that $\tilde{\kappa}_i^n$ is always negative. This requires a constraint on the time step (called past-shield condition):

$$\Delta t \leq \min_T \min_{i \in T} \frac{2|T|}{3\kappa_i^+} \tag{29}$$

Under this condition it is possible to distribute the residual Φ^K only to the nodes of the level $n+1$:

$$\begin{cases} \Phi_i^n = 0 \\ \Phi_i^{n+1} = \beta_i \Phi^K \end{cases}$$

The extension of LDA scheme to the space-time framework is straightforward. The distribution coefficients are defined with the space-time upwind parameters:

$$\beta_i^{\text{LDA}} = \frac{\tilde{\kappa}_i^{n+1,+}}{\sum_{j \in T} \tilde{\kappa}_j^{n+1,+}} \tag{30}$$

From here, everything stays the same as for the steady problem. After the distribution of the residual, we assemble all the contributions to each node into the nodal Eq. (11). This system of equations is solved by pseudotime iterations [Eq. (12)], which after convergence provides the solution at the new time step $n+1$.

High-Order Discretization

We use the approach of Ricchiuto et al. [21] and Villedieu et al. [22] to extend space-time schemes to high-order discretization. To provide high order of accuracy both in space and in time, we combine quadratic triangular elements in space with a quadratic discretization of time. This means that each triangular element in space is equipped with 6 degrees of freedom. We split this triangle in four subelements $\{T_s\}_{s=1,4}$ like on Fig. 6a. This yields the new space-time prism of Fig. 6b that has three levels in time. Each level is composed of quadratic triangles in space. In this prism, u is approximated in the same way as before, by Eq. (25), where $\psi_i(x,y)$ now denotes the (mesh dependent) quadratic continuous Lagrangian basis function, and H^l is the 1-D (time dependent) quadratic basis function. We split this prism in subprisms based on the subelements of the *quadratic* triangle (as illustrated on Fig. 6b). In each of this subprism we can still define the space-time upwind parameters in the same way as for the linear elements [Eq. (13)] but now the upwind parameter k_i is defined with the scaled normals of the subtriangle T_s. At each time iteration u^{n-1} and u^n are known and we want to compute u^{n+1} using the usual steps. First, we compute the residual on each subprism between t^{n+1} and t^n:

$$\Phi^{K_s} = \int_{t_n}^{t_{n+1}} \int_{T_s} \left(\frac{\partial u^h}{\partial t} + \nabla \cdot \boldsymbol{\mathcal{F}}^h - S \right) \mathrm{d}\Omega \, \mathrm{d}t$$

Then, the residual is distributed to all the nodes of the subtriangle T_s of the level $n+1$ and we assemble the nodal contributions. Finally, we use pseudotime iterations to solve the final system as before.

System of Equations

The unsteady solution to a system of equations is considered:

$$\frac{\partial \mathbf{U}}{\partial t} + \nabla \cdot \boldsymbol{\mathcal{F}}(\mathbf{U}) = \mathbf{S}, \quad \forall\ (x,y) \in \Omega \tag{31}$$

where $\mathbf{U}$ is the m-vector of the conserved quantities, and $\mathcal{F}$ is a $m \times 2$-tensor: $\boldsymbol{\mathcal{F}} = (\mathbf{F}, \mathbf{G})$, $\mathbf{F}$ and $\mathbf{G}$ being m-vectors. We denote by (A, B) the jacobian of $\boldsymbol{\mathcal{F}}$ in the x- (resp. y-) directions. $\mathbf{S}$ represents the vector of the source terms. In particular, it represents the monopole, dipole,... sources when considering acoustic test cases. The space-time domain is discretized like described in the previous sections. Each of the subprisms is equipped with a set of space-time upwind matrices:

$$\tilde{K}_i^{n+1} = \frac{|T_s|}{3} I + \frac{\Delta t}{2} K_i^{n+1} \tag{32}$$

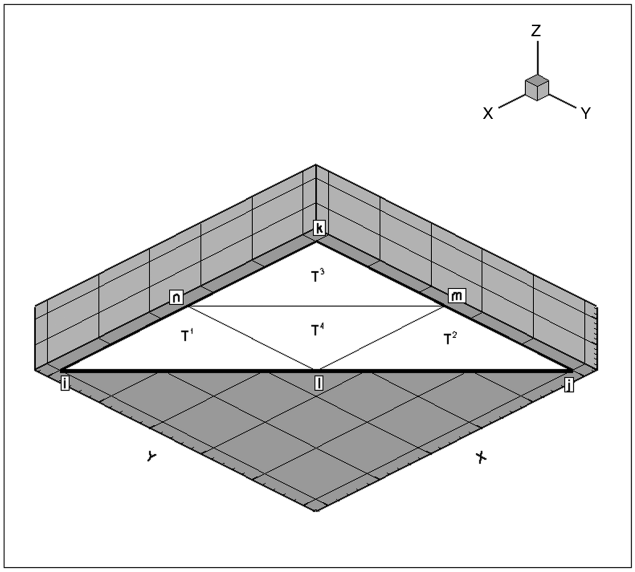

a) Quadratic elements in space

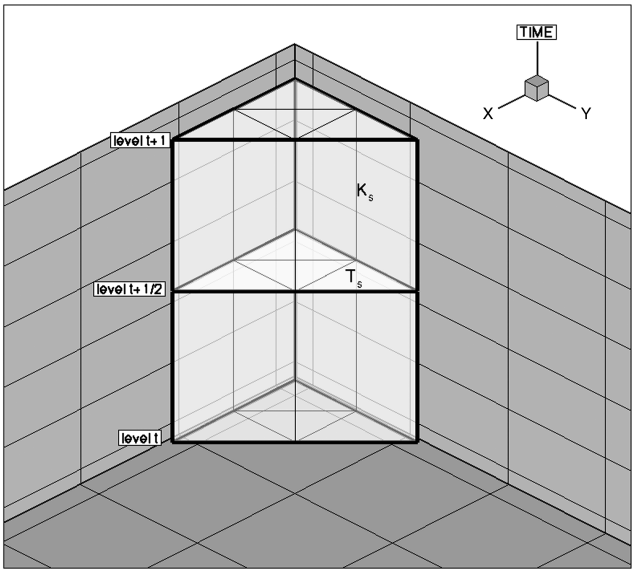

b) Quadratic space-time element

Fig. 6 High-order elements.

where I is the identity matrix and K_i^{n+1} is the space upwind matrix of the level $n+1$ defined by:

$$K_i^{n+1} = An_i^x + Bn_i^y \tag{33}$$

Since we consider a hyperbolic system of equations, $\tilde{K}_i^{n+1}$ admits a complete set of eigenvectors and eigenvalues. In case of Euler-type equations (like the later used LEEs in this paper) these eigenvalues represent the propagation speed of the characteristic waves defining the solution. So, we can define upwinding along these propagation directions and set $\tilde{K}_i^{n+1,\pm}$, the positive and negative part of $\tilde{K}_i^{n+1}$, by:

$$\tilde{K}_i^{n+1,\pm} = R_i \Lambda_i^{\pm} R_i^{-1} \tag{34}$$

where R_i is the matrix of the right eigenvectors of $\tilde{K}_i^{n+1}$ and $\Lambda_i^{\pm}$ the diagonal matrix of the positive (resp. negative) part of its eigenvalues. We also define N by:

$$N = \left(\sum_{i \in T_s} \tilde{K}_i^{n+1,+} \right)^{-1} \tag{35}$$

The matrix N always exists for a symmetric hyperbolic linear system. We refer to Abgrall [23] for the general case. The method follows exactly the same steps as usually. First, we compute the space-time residual on each (sub-)prism:

$$\mathbf{\Phi}^{K_s} = \int_{t_n}^{t_{n+1}} \int_{T_s} \left(\frac{\partial \mathbf{U}^h}{\partial t} + \nabla \cdot \boldsymbol{\mathcal{F}}^h - \mathbf{S}^h \right) \mathrm{d}\Omega \, \mathrm{d}t$$

Considering that the extension of the past-shield condition to matrix-schemes is respected we distribute the residual to all nodes of the (sub-)triangle of level $n+1$

$$\mathbf{\Phi}_i^{n+1} = B_i \mathbf{\Phi}^{K_s}$$

where B_i is the distribution matrix. As in the scalar case, the system extension of LDA scheme is considered in this work:

$$B_i = (\tilde{K}_i^{n+1,+})N \tag{36}$$

In particular, the past-shield condition needs to be adapted to system of equations. It reads now:

$$\Delta t \leq \min_{T_s \in \tau_h} \min_{i \in T_s} \frac{2|T_s|}{3\rho(K_i^+)} \tag{37}$$

where $\rho(.)$ represents the largest eigenvalue in absolute value of a matrix. Finally, we assemble all the contributions to each node and we solve:

$$\sum_{T_s, i \in T_s} \mathbf{\Phi}_i^{n+1} = 0$$

using the same iterative methods discussed in the scalar case.

Application to Linear Wave Propagation

The previously described method is proposed for noise propagation problems. First an analytical derivation was performed to explore the properties of the discretization method if periodic wave-excitation is considered. After, the derivation is justified by numerical experience and finally, some basic problems are simulated.

Fourier-Type Wave Propagation Analysis

Aerodynamically generated noise, and noise in general, is a decomposition of different sound wave modes. Thus, any numerical method used to compute noise generation and/or propagation must be able to represent these modes and their propagation. An important constrain for the numerics is that the numerical dissipation and dispersion error must be as small as possible for all the relevant modes. Therefore, it is necessary to perform a wavelength based numerical analysis to identify the limits of the chosen discretization technique.

Semidiscrete analysis of the space operator in one dimension. First, the dissipation and dispersion relation of the 1-D spatial discretization with LDA scheme is considered. The aim of this separate space analysis is to validate the applied method. In one dimension all the three basic numerical methods (FDM, FVM and FEM) are equivalent, so, often the finite difference framework is used for analyzing numerical schemes [24]. However this approach is not applicable for RDM since it cannot take into account the multidimensionality which is one of the most important feature of the applied method. So, in general, a 1-D analysis is not able to characterize the method, but it is a good way to validate the analysis procedure. Knowing that in 1D the LDA scheme is reducing to first-order upwind scheme, the analysis should give back the dissipation and dispersion relation which belong to such a scheme.

Let consider the one-dimensional scalar unsteady advection equation:

$$\frac{\partial u}{\partial t} + a \frac{\partial u}{\partial x} = 0 \tag{38}$$

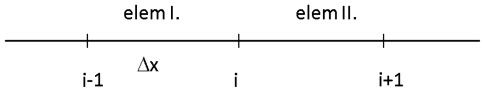

Fig. 7 1-D grid in space.

and a harmonic perturbation of the form:

$$u(t,x) = \hat{u} \cdot e^{\iota(kx - \omega t)} \tag{39}$$

The aim of the analysis is to compare how the discrete and exact problem respond to this perturbation. Now, we consider only the space discretization combined with exact time integration. Then, the resiudal of Eq. (38) on a uniform grid (Fig. 7) needs to be compared with the analytical solution $k^{\text{exact}} = \omega / a$. The 1-D prototype element and its characteristics are summarized in Fig. 8.

In case of P1 elements the residual over an element can be expressed as [Eq. (9)]:

$$\Phi^T = \sum_T \kappa_i u_i \tag{40}$$

The residuals of the two elements containing node i then read:

$$\Phi^{\mathrm{I}} = \kappa_1 u_{i-1} + \kappa_2 u_i = a(u_i - u_{i-1}) \tag{41}$$

$$\Phi^{\mathrm{II}} = \kappa_1 u_i + \kappa_2 u_{i+1} = a(u_{i+1} - u_i) \tag{42}$$

After distribution, the sum of the distributed residuals belonging to node i is:

$$\Phi_i = \Phi^{\mathrm{I}} = a(u_i - u_{i-1}) \tag{43}$$

To validate the analysis method developed for RDM, we are using the equivalence between Petrov–Galerkin Method [25] and RDM. The time derivative can be expressed as:

$$-\Phi_i = 2 \int_E \psi_i \frac{\partial u}{\partial t} \, \mathrm{d}E \tag{44}$$

where ψ_i is the one-dimensional linear continuous Lagrangian basis function. This type of time discretization is just a choice and it is irrelevant as far as only the space analysis is considered. It is worth to note, that a systematic space analysis cannot be done like in case of RDM since the unsteady discretization is not straightforward as explained previously. Inserting Eq. (39) to this residual [Eq. (44)] gives:

$$-\Phi_i = -\iota \omega u_i \Delta x = -a(1 - e^{\iota k \Delta x}) \tag{45}$$

The numerical wavenumber then can be expressed as:

$$k^{\text{num}} = \frac{\omega}{a} = \frac{\iota}{\Delta x}(e^{\iota k \Delta x} - 1) \tag{46}$$

The complex amplification factor $G(k\Delta x)$ finally gives the dispersion and dissipation properties of the spatial discretization

$$G(k\Delta x) = \frac{k^{\text{num}}}{k^{\text{exact}}} = \frac{\iota}{k\Delta x}(e^{\iota k \Delta x} - 1) \tag{47}$$

In Fig. 9 the numerical dispersion and dissipation relation is given for P1 RDM-LDA scheme, FDM first- and second-order scheme with the exact solution. As expected, in 1D the LDA scheme reduces to first-order upwind scheme, resulting in a stable scheme due to its

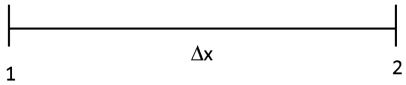

$$k_1 = -a \quad \beta_1 = 0$$
$$k_2 = a \quad \beta_2 = 1$$

Fig. 8 1-D prototype element.

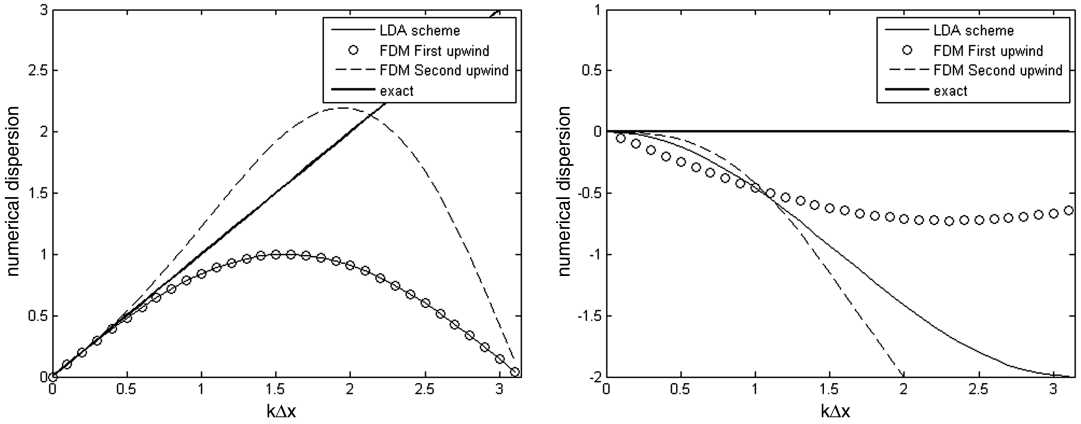

a) Numerical dispersion **b) Numerical dissipation**

Fig. 9 Numerical dispersion and dissipation due to space discretization in 1-D.

in-built numerical dissipation (Fig. 9, right side) high for almost all the wave-numbers.

Mass-Matrix Discretization Analysis in 1D: In the previous analysis perfect time integration was assumed. The full residual (space + time) in case of mass-matrix time integration can be computed according to Eq. (23).

In the 1-D linear case the additional term reads as:

$$\Phi_i^{MM} = \sum_{j\in T} m_{ij}(u_j^{n+1} - u_j^n) = \frac{1}{6}\Delta x[(u_{i-1}^{n+1} - u_{i-1}^n) + 2(u_i^{n+1} - u_i^n) + u_{i+1}^{n+1} - u_{i+1}^n] \tag{48}$$

So, the full residual due to the space and time integration can be assembled as:

$$\Phi_i = \Phi_i^{MM} + \Phi_i^{\text{Space}} \tag{49}$$

where Φ_i^{Space} is the residual due to the space discretization:

$$\Phi_i^{\text{Space}} = a(u_i^n - u_{i-1}^n) + a(u_i^{n+1} - u_{i-1}^{n+1}) \tag{50}$$

In the full analysis we are seeking a solution in the form:

$$u(t,x) = \hat{u} \cdot e^{\iota(ik\Delta x - n\omega\Delta t)} \tag{51}$$

If the parts containing the variables from the time level n and time level $n+1$ are separated then, the response of the discretization to planar wave-excitation can be expressed:

$$\Phi_i^{n+1} = \frac{1}{6}\Delta x[u_{i-1}^{n+1} + u_i^{n+1} + u_{i+1}^{n+1}] + (\Phi^{\text{Space}})^{n+1} = e^{\iota\omega\Delta t} \cdot l(k\Delta x) \tag{52}$$

$$\Phi_i^n = -\frac{1}{6}\Delta x[u_{i-1}^n + u_i^n + u_{i+1}^n] + (\Phi^{\text{Space}})^n = m(k\Delta x) \tag{53}$$

$$e^{\iota\omega\Delta t} = \frac{m(k\Delta x)}{l(k\Delta x)} \tag{54}$$

where l and m are known functions of $k\Delta x$.

The dissipation and dispersion relation corresponding to the full mass-matrix type discretization can be seen in Fig. 10. Likewise most unsteady methods, as Δt reduces (so the Courant–Friedrichs–Lewy, or CFL, number $\nu = \frac{a\Delta t}{\Delta x}$ getting smaller and smaller) the discretization performs better, resulting less dissipation and wider range of resolved frequencies. In Table 1 the number of nodes needed to resolve one wavelength is presented for few CFL numbers in case of mass-matrix type discretization. As we can see, due to the introduction of time discretization (which introduces one more approximation) the performance reduces. For $\nu = 1.0$ we need more nodes/wavelengh than in case of pure space discretization. As ν reduces the performance increases and gets better than reported by the semidiscretized analysis. However, in general, it is preferred to have as high time step as possible to reduce computational cost, so the unlimited reduction of Δt is not possible for practical applications.

Space-Time Discretization Analysis in 1-D: Now, the whole analysis is repeated for the 1-D space-time discretization on prismatic elements. The steps are the same as for the space operators,

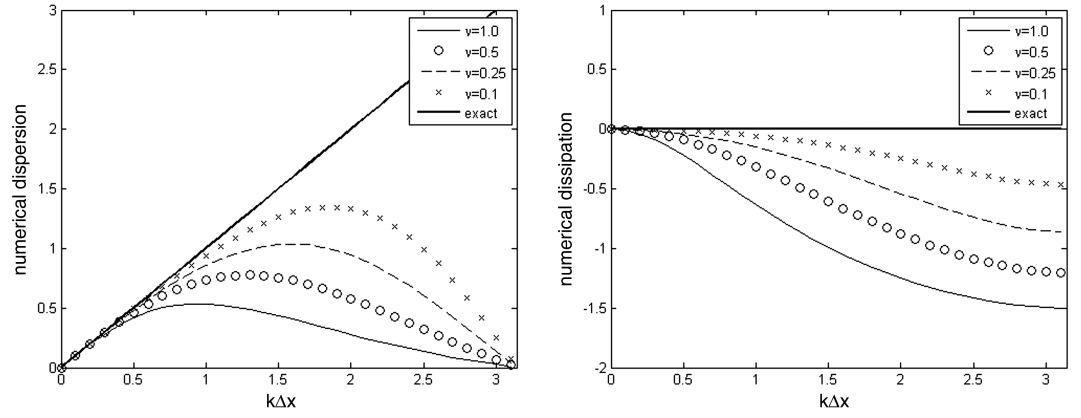

a) Numerical dispersion **b) Numerical dissipation**

Fig. 10 Numerical dispersion and dissipation due to mass-matrix type discretization in 1-D in the function of ν.

Table 1 Number of nodes/wavelength needed in case of mass-matrix type time discretization

ν	NPW
1.0	31
0.5	18
0.25	10
0.1	8

Table 2 Number of nodes/wavelength needed in case of space-time type time discretization

ν	NPW
1.0	13
0.75	8
0.55	6
0.35	8

but now 2-D prismatic elements are considered, where the second dimension is the time (Fig. 11).

There is one prototype element again with the properties depicted in Fig. 12. The maximum time-step size Δt is limited by the past-shield condition, i.e., the past cannot be affected by the future. In this sense β_1 and β_2 has to be zero, which gives the condition $\nu < 1$.

The residual due to the space-time discretization over the elements involving node (t, i) reads as follows:

$$\Phi^{\mathrm{I}} = \kappa_1 u_{t-1,i-1} + \kappa_2 u_{t-1,i} + \kappa_4 u_{t,i-1} + \kappa_3 u_{t,i} \tag{55}$$

$$\Phi^{\mathrm{II}} = \kappa_1 u_{t-1,i} + \kappa_2 u_{t-1,i+1} + \kappa_4 u_{t,i} + \kappa_3 u_{t,i+1} \tag{56}$$

The distributed residual belongs to node (t, i):

$$\Phi_{t,i} = \beta_3 \Phi^{\mathrm{III}} + \beta_4 \Phi^{\mathrm{IV}} \tag{57}$$

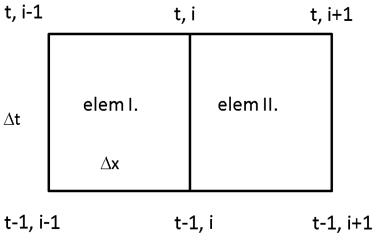

Fig. 11 1-D grid space-time grid.

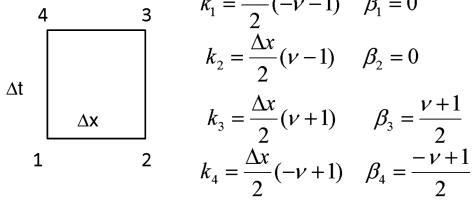

Fig. 12 1-D space-time prototype element.

Substituting Eq. (51) to Eq. (57) we get the amplification factor for the 1-D full space-time discretization in the function of the CFL number ν. The space-time RDM does not follows the same trend as all the other methods, as can be seen in Fig. 13. There is an optimal time-step range around $\nu \approx 0.55$.

Because of the space-time formulation, with the optimal CFL = 0.55 number it is enough to have:

$$\mathrm{NPW} = \frac{2\pi}{(k\Delta x)_{\max}} \approx 6 \tag{58}$$

nodes per wave number, but still with using a compact stencil. In Table 2 the number of nodes/wavelength is given for some CFL numbers.

Semidiscrete Analysis of the Space Operator in 2-D: An important feature of RDM is the possibility build multidimensional upwinding schemes. The objective of the 2-D analysis is to see the impact of multidimensional upwinding on the dispersion and dissipation. First, a 2-D space discretization analysis is performed, after the full space-time system is investigated.

Let consider a 2-D scalar advection problem:

$$\frac{\partial u}{\partial t} + \mathbf{a} \cdot \nabla u = 0 \tag{59}$$

Let suppose that the solution is periodic over the domain $[0, L]^2$, the grid spacing is Δx for both directions and the domain is discretized by a uniform triangulation (Fig. 14). Again, we are looking for the response of the numerical discretization due to the following excitation:

$$u(t, x, y) = \hat{u} \cdot e^{\imath(k_x x + k_y y - \omega t)} \tag{60}$$

So, the solution of Eq. (59) is the superposition of planar waves. Then, it is enough to determine the response of the discretization method to one single mode. The exact solution of such a harmonic excitation is:

$$\omega = \mathbf{k} \cdot \mathbf{a} \tag{61}$$

where $\mathbf{k} = [k_x k_y]^T$. In 2-D, as shown in Fig. 15, there is two prototype elements. The upwind parameters κ define which nodes are in the

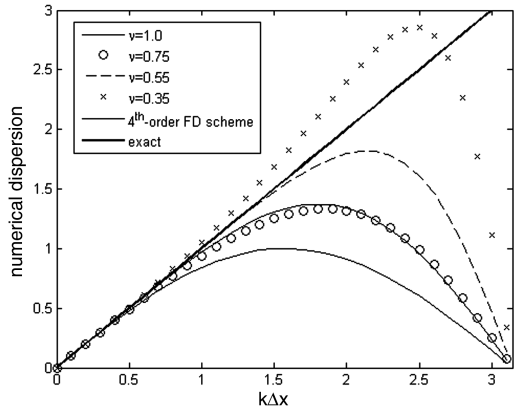

a) Numerical dispersion

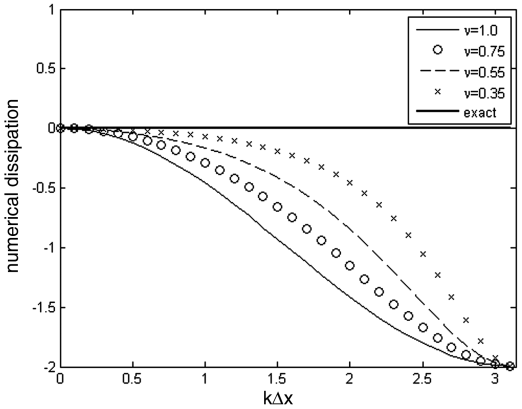

b) Numerical dissipation

Fig. 13 Numerical dispersion and dissipation due to space-time discretization in 1-D in the function of ν.

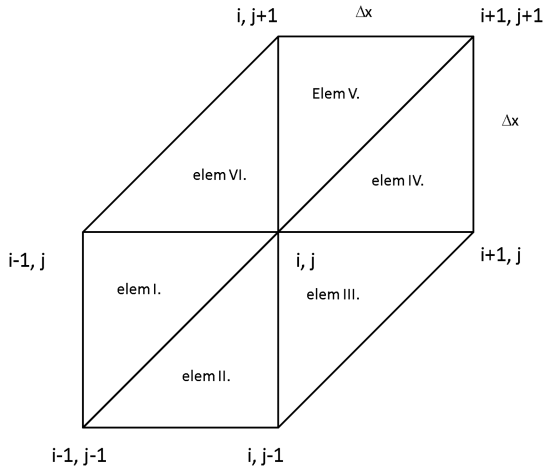

Fig. 14 2-D grid in space.

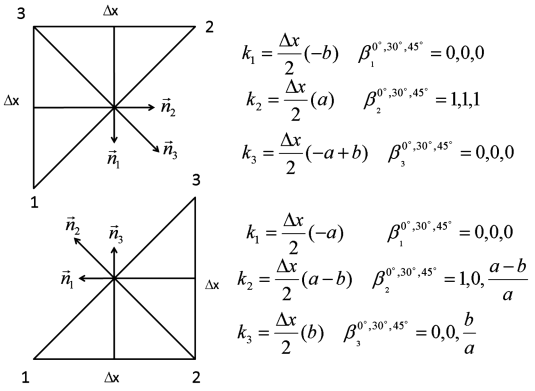

Fig. 15 2-D prototype elements.

upwind or downwind direction. In case of the LDA scheme, thanks to its multidimensional upwinding property, the residual is distributed to the downwind nodes along the streamlines. The residuals of the involving elements are computed the same way as before:

$$\Phi^E = \sum_E \kappa_i u_i \tag{62}$$

Seek for the solution in the form:

$$u(t,x,y) = \hat{u} \cdot e^{\imath(ik_x\Delta x + jk_y\Delta y - \omega t)} \tag{63}$$

The results are shown in Fig.16. It is less dissipative for the high wave-numbers, however, its dispersion relation is much less than the one of the first-order finite difference one. Of course, the dispersion relation do not affect the steady solution. The question is then if the upwinding improves such dramatically the performance of the RDM as in case of 1D, and moreover, if the optimal CFL number depends on the number of dimensions and/or on the grid topology.

Space-Time Discretization Analysis in 2-D: When the full two-dimensional space and time discretization is considered we are looking for the solution in the form:

$$u(t,x,y) = \hat{u} \cdot e^{\imath(ik_x\Delta x + jk_y\Delta y - n\omega\Delta t)} \tag{64}$$

Now, we use the prismatic elements introduced in Fig. 5, so the upwind parameters have to be modified accordingly:

$$\kappa_i^n = \frac{\Delta t}{2}\kappa_i - \frac{|T|}{3} \qquad \kappa_i^{n+1} = \frac{\Delta t}{2}\kappa_i + \frac{|T|}{3} \tag{65}$$

where κ_i is the space upwind parameter of node i. Otherwise the computation of the residual and the distribution follows the same pattern as in the previous cases. The dispersion and the dissipation along the streamlines due to the whole discretization (flow angle $\alpha = 30°$, CFL number $\nu = 0.6$) can be seen in Fig. 17. The space-time formulation preserved the characteristic of the space discretization, but improved its performance just like in 1D. Even in the 2-D case with flow not aligned with the grid, the optimal CFL number is the same as for the 1-D case, indicating that it is not dependent on the dimension of the problem nor on the grid itself. The minimum number of gridpoints that has to be used over a wavelength is the same as well (NPW = 6).

LEEs

In the present work we consider the LEEs in two spatial directions, as derived by Bailly and Juvé [26] for inhomogeneous mean flow, written in conservative variables:

$$\begin{aligned}
&\frac{\partial \rho'}{\partial t} + \frac{\partial}{\partial x_j}(\rho_0 u_j' + \rho' u_{0j}) + \frac{\partial}{\partial x_j}(\rho_0 u_j' + \rho_0 u_{0j}) = 0 \\
&\frac{\partial \rho_0 u'}{\partial t} + \frac{\partial}{\partial x_j}(\rho_0 u_i' u_{0j} + p'\delta_{ij}) + \frac{\partial u_{0i}}{\partial x_j}(\rho_0 u_j' + \rho' u_{0j}) \\
&\quad + \left\{\frac{\partial \rho' u'}{\partial t} + \frac{\partial}{\partial x_j}(\rho' u_i' u_{0j} - \overline{\rho' u_i'} u_{0j}) + \frac{\partial u_{0i}}{\partial x_j}(\rho' u_j' - \overline{\rho' u_j'})\right\} \\
&\quad = \left\{-\frac{\partial}{\partial x_j}(\rho_0 u_i' u_j' - \overline{\rho_0 u_i' u_j'})\right\} \\
&\frac{\partial p'}{\partial t} + \frac{\partial}{\partial x_i}(\gamma(p_0) u_i' + p' u_{0i}) + (\gamma - 1)\left(p'\frac{\partial u_{0i}}{\partial x_i} - u_i'\frac{\partial p_0}{\partial x_i}\right) \\
&\quad + \left\{u_i'\frac{\partial p'}{\partial x_i} - \overline{u_i'\frac{\partial p'}{\partial x_i}}\right\} = 0
\end{aligned} \tag{66}$$

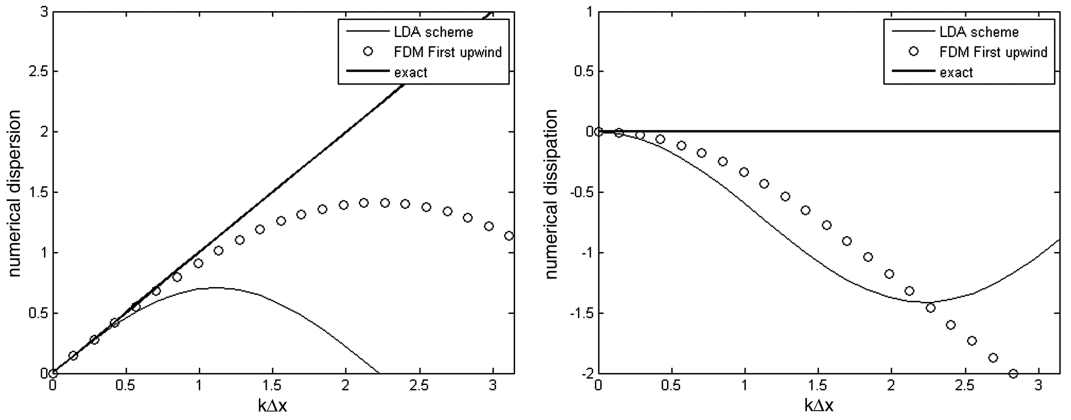

a) Numerical dispersion **b) Numerical dissipation**

Fig. 16 Numerical dispersion and dissipation due to space discretization in 2-D plotted along the streamlines.

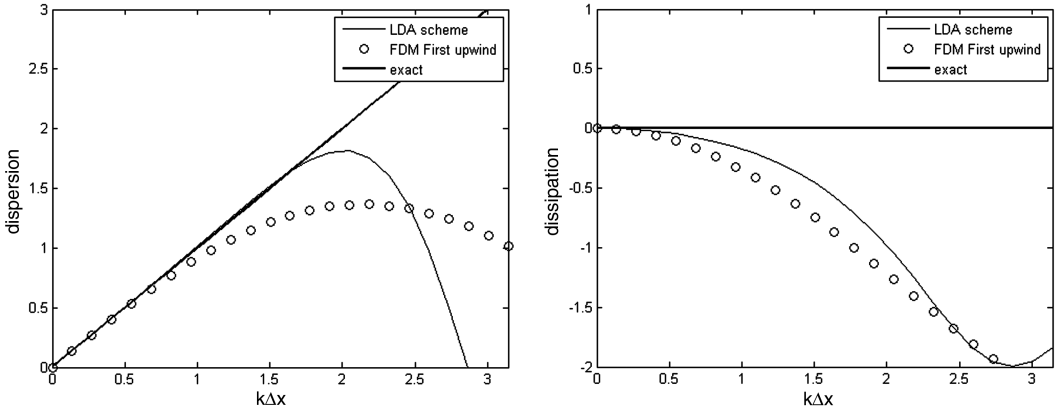

a) Numerical dispersion **b) Numerical dissipation**

Fig. 17 Numerical dispersion and dissipation due to space-time discretization in 2-D.

The terms subscripted with 0 are time-averaged mean flow quantities that are known functions (available for example from a RANS calculation). The variables with prime are the fluctuating perturbations, and so the unknowns. The overbar denotes time averaging. The terms containing the multiplication of the fluctuations are small, and therefore they are neglected (in $\{\}$). In the present implementation finally the following set of partial differential equations (in matrix notation) is discretized:

$$\frac{\partial \mathbf{U}}{\partial t} + \frac{\partial \mathbf{F}}{\partial x} + \frac{\partial \mathbf{G}}{\partial y} + \mathbf{H} = \mathbf{S} \tag{67}$$

Since the LEE are a linear set of equations, Eq. (67) can be rewritten as:

$$\frac{\partial \mathbf{U}}{\partial t} + \mathbf{A}\frac{\partial \mathbf{U}}{\partial x} + \mathbf{B}\frac{\partial \mathbf{U}}{\partial y} + \mathbf{H} = \mathbf{S} \tag{68}$$

The vectors and matrices read as follows:

$$\mathbf{U} = \begin{bmatrix} \rho' \\ \rho_0 u' \\ \rho_0 v' \\ p' \end{bmatrix}, \qquad \mathbf{A} = \frac{\partial \mathbf{F}}{\partial \mathbf{U}} = \begin{bmatrix} u_0 & 1 & 0 & 0 \\ 0 & u_0 & 0 & 1 \\ 0 & 0 & u_0 & 0 \\ 0 & c_0^2 & 0 & u_0 \end{bmatrix}$$

$$\mathbf{B} = \frac{\partial \mathbf{G}}{\partial \mathbf{U}} = \begin{bmatrix} v_0 & 0 & 1 & 0 \\ 0 & v_0 & 0 & 0 \\ 0 & 0 & v_0 & 1 \\ 0 & 0 & c_0^2 & v_0 \end{bmatrix}$$

$$\mathbf{H} = \begin{bmatrix} 0 \\ (\rho' u_0 + \rho_0 u')\frac{\partial u_0}{\partial x} + (\rho' v_0 + \rho_0 v')\frac{\partial u_0}{\partial y} \\ (\rho' u_0 + \rho_0 u')\frac{\partial v_0}{\partial x} + (\rho' v_0 + \rho_0 v')\frac{\partial v_0}{\partial y} \\ (\gamma-1)p'\left(\frac{\partial u_0}{\partial y} + \frac{\partial v_0}{\partial x}\right) - (\gamma-1)\left(u'\frac{\partial p_0}{\partial x} + v'\frac{\partial p_0}{\partial y}\right) \end{bmatrix}$$

S can represent the acoustic sources such as monopole, dipole, etc. Bailly and Juvé [26] reported that growing instability waves can be excited by source terms in LEE through the mean shear. To prevent the development of linear instability waves the terms containing the derivatives of the background flow **H** are treated as source terms and artificial numerical filtering is applied, if growing high-frequency waves are observed in the solution [27].

At the boundaries Thompson's nonreflective boundary conditions are used [28]. This boundary treatment rely on the characteristic theory. It is well known [29] that the number of physical conditions that have to be prescribed at the boundary depend on the sign of the eigenvalues of the characteristic system. Only the information coming from outside has to be imposed, all the others are provided naturally by the inner domain. In the case of acoustic problems the first difficulty arising is to know what kind of conditions should be fixed. In the present LEEs, the solution variables are the fluctuations of density, velocity, and pressure. At an inflow boundary condition three of them should be given, for an outflow just one. But none of the conservative variables are known, in general. It is much easier acting on the waves themselves.

To impose boundary conditions for the characteristic waves, first the conservative variables have to be transformed to characteristic ones locally at the boundaries. The characteristic matrix of the LEE (67) in two spatial dimension can be constructed as follows:

$$\mathbf{D} = \mathbf{A}\cdot n_x^{\text{char}} + \mathbf{B}\cdot n_y^{\text{char}} = \begin{bmatrix} U_n & n_x^{\text{char}} & n_y^{\text{char}} & 0 \\ 0 & U_n & 0 & n_x^{\text{char}} \\ 0 & 0 & U_n & n_y^{\text{char}} \\ 0 & c^2\cdot n_x^{\text{char}} & c^2\cdot n_y^{\text{char}} & U_n \end{bmatrix}$$

where $U_n = u_0\cdot n_x^{\text{char}} + v_0\cdot n_y^{\text{char}}$, and the characteristic matrix (and later the variables as well) are defined by the characteristic normal vector $\mathbf{n}^{\text{char}} = [n_x^{\text{char}} n_y^{\text{char}}]^T$. The eigenvalues of the matrix **D** can be calculated by solving the algebraic equation:

$$\det|\mathbf{D} - \lambda\mathbf{I}| = 0 \tag{69}$$

resulting in:

$$\boldsymbol{\lambda} = \begin{bmatrix} U_n \\ U_n \\ U_n + c \\ U_n - c \end{bmatrix}$$

In the case of Euler-type equations the eigenvalue U_n has a multiplicity equal to the number of the space dimensions. For a one-dimensional case a unique definition of the eigienvectors are possible, while in two and three dimensions different choices are possible. The left eigenvectors of the matrix **D** based on the characteristic normal vector can be obtained solving:

$$\mathbf{L}\mathbf{D} = \Lambda\mathbf{L} \tag{70}$$

where Λ is a diagonal matrix with the eigenvalues in the diagonal. The matrix of the right eigenvectors can be obtained as $\mathbf{R} = \mathbf{L}^{-1}$. The characteristic variables defined as:

$$\partial\mathbf{W}_n = \mathbf{L}\cdot\partial\mathbf{U} = \begin{bmatrix} \partial\rho' - \partial\frac{p'}{c^2} \\ \partial\rho_0\cdot\mathbf{s}\mathbf{u}' \\ \partial\rho_0\cdot\mathbf{n}^{\text{char}}\mathbf{u}' + \partial\frac{p'}{c} \\ \partial\rho_0\cdot\mathbf{n}^{\text{char}}\mathbf{u}' - \partial\frac{p'}{c} \end{bmatrix} = \begin{bmatrix} S \\ \Omega \\ A^+ \\ A^- \end{bmatrix}$$

Here $\mathbf{s}$ is a normal vector parallel to $\mathbf{n}^{\text{char}}$. The characteristic variables represent in two spatial dimension the four information waves travelling through the domain: 1) S: entropy wave, 2) Ω: shear wave, 3) A^+: positive acoustic wave, and 4) A^-: negative acoustic wave.

These waves travel with the speed defined by the corresponding eigenvalues: the entropy and the shear waves transported with the mean flow U_n and the acoustic waves convected by $U_n \pm c$. It is worth mentioning that the characteristic variables depend on the choice of the normal vector $\mathbf{n}$. This choice of the characteristic normal vector $\mathbf{n}^{\text{char}}$ is not trivial in element-based discretization. The characteristic normal vector cannot be the face normal vector (which would be a trivial choice if boundary conditions are considered) since it would result in a discontinuous representation of the variables. To overcome this difficulty the solver is implemented in conservative variables and then locally transformed to characteristic variables to impose boundary conditions on them. In the present work the inflow and outflow boundary conditions are considered and both boundary conditions are implemented in strong and weak form.

The weak boundary formulation is inspired by the "ghost-cell" approach used in finite volume method, and its advantage is that the interior schemes can be used at the boundary nodes [30]. In this case the boundary restriction just softly applied on the boundary, which tended to be the desired value as the number of subiterations advanced. At the boundary, ghost-cells are attached to the boundary elements (Fig. 18a). The solutions in 1* and 3* are defined as follows: 1) $S_{1*} = S_{3*} = S_i$, 2) $\Omega_{1*} = \Omega_{3*} = \Omega_i$, 3) $A^+_{1*} = A^+_{3*} = A^+_i$, and 4) $A^-_{1*} = A^-_{3*} = A^-_i$.

Here, S, Ω, A^+, and A^- denotes the characteristic variables, the entropy, vorticity, and positive/negative acoustic waves [28]. In the next step the geometrical location of node 1* and 3* tend to that of node i. For the triangle $T(i, 1*, 2)$ the gradient of a linear variable u is defined as:

$$2 \cdot S_T \nabla u = \sum_{j \in T} u_j \mathbf{n}_j = (u_2 - u_i) \cdot \mathbf{n}_2 + (u_{1*} - u_i) \cdot \mathbf{n}_{1*} \tag{71}$$

In the infinitely thin cell it reduces to:

$$2 \cdot S_T \nabla u = (u_{1*} - u_i) \cdot \mathbf{n}_{1*} = -(u_{1*} - u_i) \cdot \mathbf{n}_1 \tag{72}$$

Therefore, the gradient and the scalar residual $\Phi_T = S_T \cdot \boldsymbol{\lambda} \nabla u$ remains finite although the cell area vanishes. In this way the wave decomposition reduces to a one-dimensional flux difference splitting between 1* and i in the direction normal to the boundary $\mathbf{n}_1$.

At the outflow in case of subsonic flowfield three eigenvalues are positive and therefore just one wave is entering to the domain (A^-). To avoid spurious reflections this wave should not enter to the domain. Wave is defined as the change of amplitude of a variable in time, therefore the derivative of A^- with respect to time should be set to zero, not just the magnitude (so the variable) resulting in a Neumann condition:

$$\frac{\partial A^-}{\partial t} = 0 \tag{73}$$

In practical implementation it means that the entropy, vorticity, and the outgoing acoustic wave is computed from the inner domain and the incoming acoustic wave is set in the ghost cells as $(A^-_{1*})^{n+1} = (A^-_{3*})^{n+1} = (A^-_i)^n$ to satisfy the condition prescribed by Eq. (73).

In the case of strong formulation the boundary condition is imposed directly on the boundary nodes. First the boundary node is handled as if it were an interior node then the residual is modified so that the boundary condition is satisfied at the nodes (Fig. 18b). In characteristic treatment the missing information is provided by a set of ingoing characteristic waves, whose intensities are computed by expressing the conditions in terms of the provisional residual.

For an explicite update scheme [Eq. (13)]:

$$u_i^{\kappa+1} = u_i^{\kappa} + \frac{\Delta\tau}{C_i} \left(\sum_{T, i \in T} \Phi_i^{a+s,T} \right)^{\kappa} \tag{74}$$

On the boundary the residual is corrected to satisfy the boundary condition imposed:

$$u_i^{\kappa+1} = u_i^{\kappa} + \frac{\Delta\tau}{C_i} \left(\sum_{T, i \in T} \Phi_i^{a+s,T} + \Phi_i^{\text{BC}} \right)^{\kappa} \tag{75}$$

Obviously, in case of outflow, for the first three waves no corrections are needed. For the incoming wave we want to satisfy Eq. (73) so the residual due to advection is set to zero with

$$\Phi_i^{\text{BC}} = -\sum_{T, iT} \Phi_i^{a+s,T}$$

The implementation has been done in the COOLFluiD [31] simulation environment which is a multiphysics code [32] developed at the von Kármán Institute.

Verification

The implementation of LEEs [Eq. (67)] will be verified using test cases having exact solution. After the analytical derivation, the characteristic of the residual distribution method for wave propagation is investigated numerically. Two simple initial value problems are considered to check the order of the LDA scheme, as well as its dissipation and dispersion properties. Then, a benchmark problem is used to test the isotropic property of the numerical solution as well as its accuracy for wave propagation. The accuracy of source resolution is shown with the simulation of a monopole in a

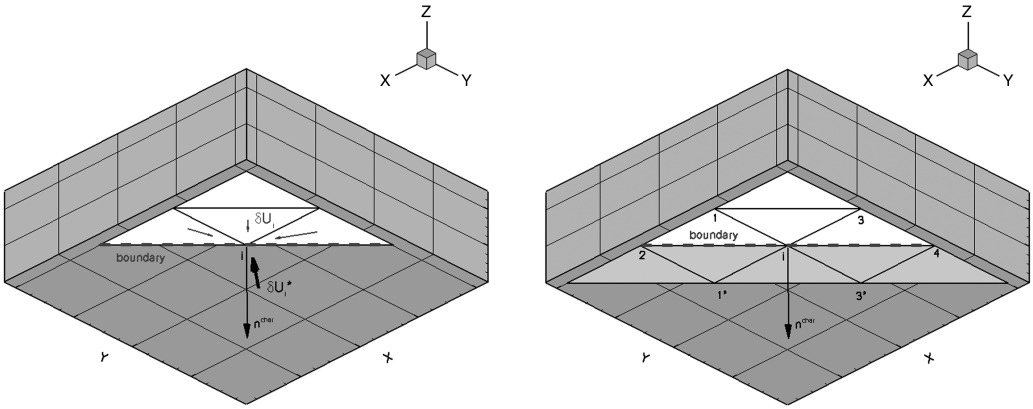

a) Strong boundary condition **b) Weak boundary condition**

Fig. 18 Practical implementaion of boundary conditions.

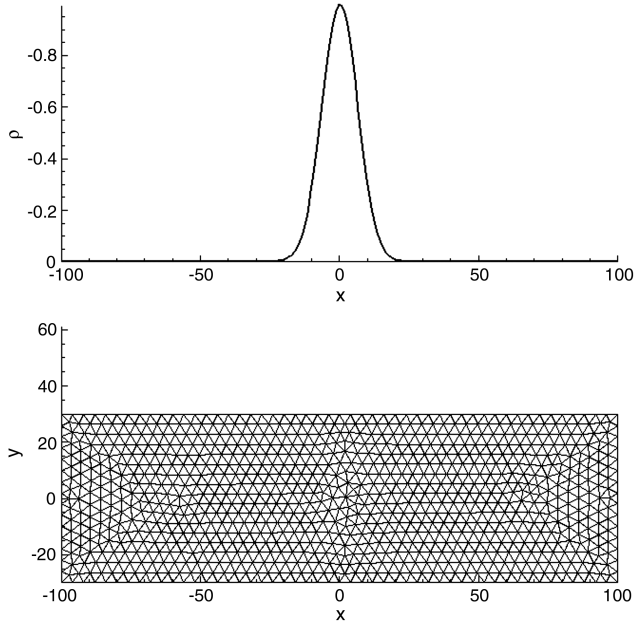

Fig. 19 Initial condition and mesh topology used in the scalarlike test case.

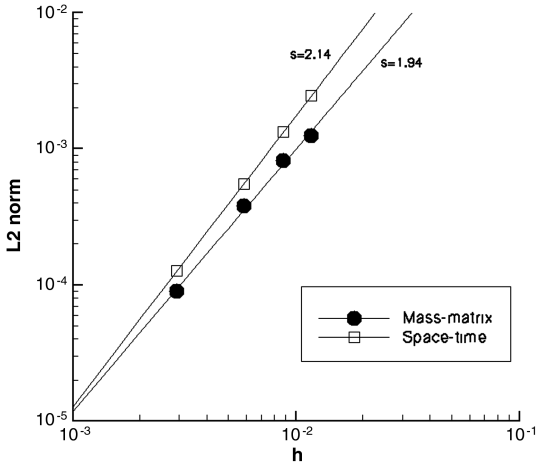

Fig. 20 Order of the mass-matrix and space-time discretization.

uniform flow. Finally, the response of the acoustic propagation in a nonuniform meanflow is investigated.

Initial Value Problems

Advection Problem: To illustrate the performance of the different time discretization methods a scalar problem was solved in the framework of LEEs. A density pulse (Fig. 19) is placed in the middle of a rectangular domain $(x, y) \in [200, 50]$ discretized by linear (P1) elements. The pulse is propagated with $M = 0.5$ through periodic boundary condition till it arrives back to its original position.

The simulation was performed on a family of unstructured grids. To go from a mesh to the following the number of nodes are devided by two. The CFL number is equal to 0.3 as a consequence of past-shield condition. The L2-norm of the result obtained with different grids are computed and plotted in Fig. 20 to get the practical order of the discretizations. It is visible that the order of the two type of discretization is the same ($s = 2.14$), however, the mass-matrix formulation perform better if the L2-norm is considered.

Analyzing the shape of the pulse at $t = 400$, so after one complete flow-through, a basic difference can be observed between the mass-matrix and the space-time discretization (Fig. 21). In general, the space-time simulation preserves more the original shape of the pulse, while the mass matrix became more amorphous. However, the mass-matrix simulation can capture the propagation speed more accurately, than the space-time method. In the results of space-time simulation the dispersion error is more displayed and increasing as the grid is getting coarser. It is hard to set up a quantitative relation as in the analytical representation, since a Gaussian pulse contain a wide range of frequencies, so with the different grid resolutions different frequency contents are resolved.

To see if the anisotropy observed in the mass-matrix solution is due to the grid topology the same entropy pulse was placed into structured triangular meshes (both right and left orientated) and advected both with the mass-matrix and the space-time formulation. The results can be seen in Fig. 22 compared with the analytical solution, as well as to the ones obtained on the unstructured mesh. Both for space-time and for mass-matrix method the orientation of the grid is affecting the solution. However, both methods keep their characteristic behavior observed on the unstructured grid. Namely, the space-time method introduces more dispersion and the mass-matrix method violate more the isotropy of the entropy pulse.

Wave Propagation Test Case: Because of the observed anisotropy and the broadband nature of the entropy pulse a second initial problem has been solved. In this case a 2-D channel is considered with a length of $L = 2\pi$ and one wavelength sinusoidal pulse is placed inside. Periodic boundary conditions are applied at the open ends of the channel. Within two periods $2T = 4\pi/c_0$ the obtained

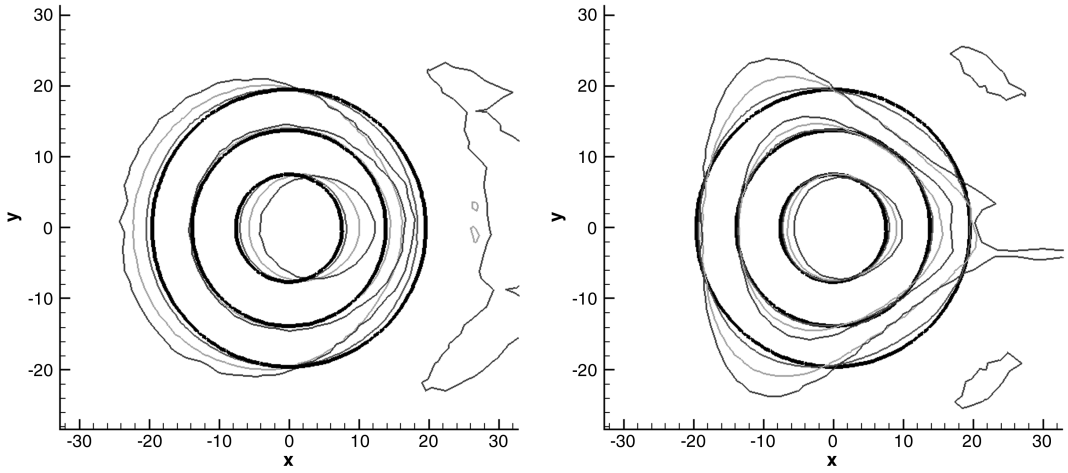

a) Space-time method **b) Mass-matrix method**

Fig. 21 Comparing the results for different grid resolutions with the exact solution. Dashed: finest grid, dotted: middle grid, solid: coarse grid, and solid-thick: exact solution. Contours of density 0.01, 0.1, 0.5.

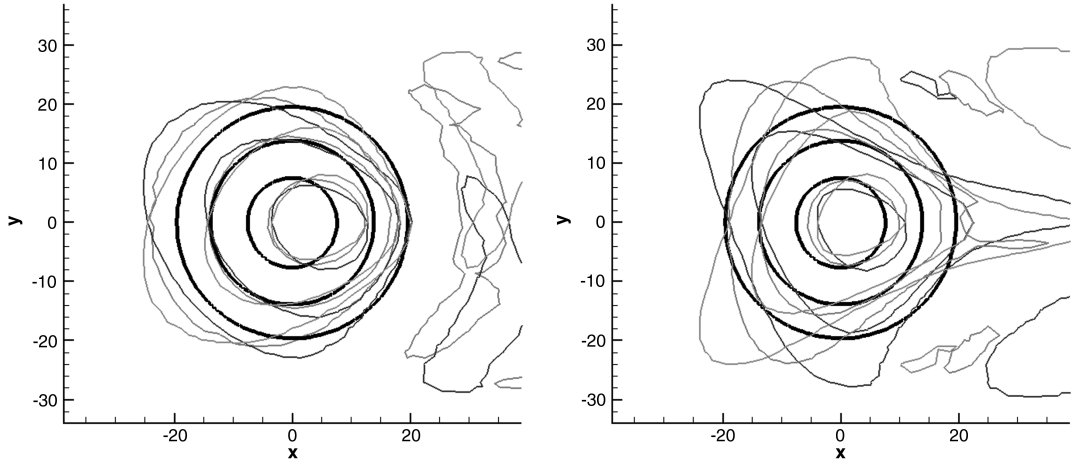

a) Space-time method **b) Mass-matrix method**

Fig. 22 Comparing the results for different grids with the exact solution. Dotted: unstructured grid, solid: left splitted grid, dashed: right splitted grid, and solid-thick: exact solution. Contours of density 0.01, 0.1, 0.5.

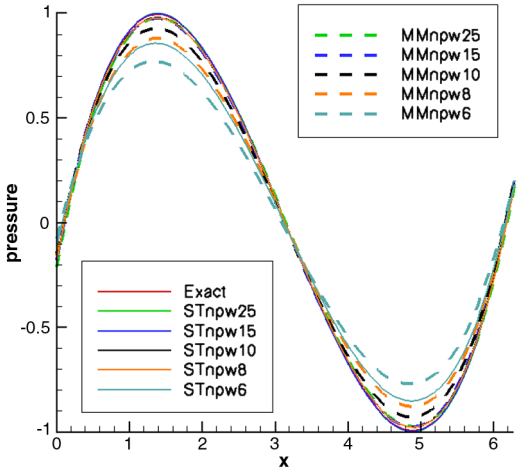

Fig. 23 Comparison of the mass-matrix method and space-time method on a sinusoidal wave propagation problem.

signal is compared with the initial condition such way the number of points per wavelength (NPW) necessary to resolve a wave can be obtained numerically. In the test five different grids were used with the resolution NPW = 6, 8, 10, 15, and 25. The CFL number was fixed to 0.3 again. Analytically, a mesh with 9–10 nodes per wavelength should be able to propagate the wave in case of the space-time discretization and with 10 for the mass-matrix type discretization. As can be seen in Fig. 23, in general, the mass-matrix formulation introduces more dissipation then the space-time method. A closer look to the top of the sinusoidal wave (Fig. 24a) shows that the space-time method can capture this wave propagation problem with a resolution of NPW = 25, 15. However, the mass-matrix method cannot recover the right amplitude with these grids.

On Fig. 24b a zoom of Fig. 23 is shown around the position $[\pi, 0]$. Looking at this point gives an indication to the dispersion error of the applied discretization. In the case of the mass-matrix method the most resolved grid (NPW = 25) gives a bit faster propagation speed than required while all the other grids propagate the acoustic wave slower then the original problem requires. The deviation from the original speed is less for the space-time method. The finest mesh gives a very good agreement to the exact solution, while the indicated other two grids (NPW = 15 and 10) still approximate the wave propagation speed well.

Benchmark Problem: Through this test case the space-time method and the mass-matrix method is compared on linear (P1) elements. The initial value problem [33] consists of an acoustic pulse centered at the origin and a combined vortex/entropy pulse placed at $(x, y) = (67.0, 0.0)$. The mean flow is uniform with Mach number $M_x = 0.5$, $M_y = 0.0$ and the time step related to CFL = 1 is $\Delta t = \frac{1}{1+M}$ (with $M = \sqrt{M_x^2 + M_y^2}$). The computational domain extends from $-100 \leq x, y \leq 100$ embedded in free space and the boundary

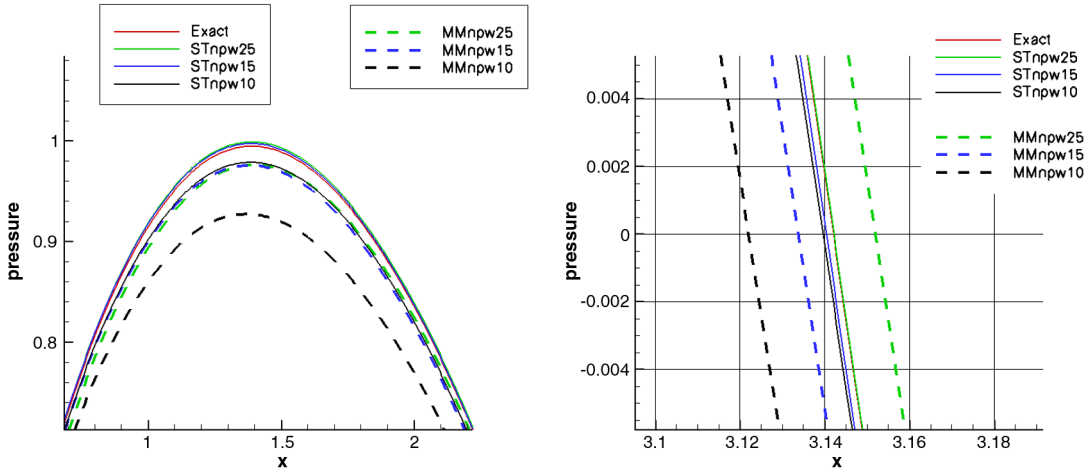

a) Top zoom **b) $y = 0$ zoom**

Fig. 24 Comparing the results for different grids with the exact solution. Zooms of Fig. 23.

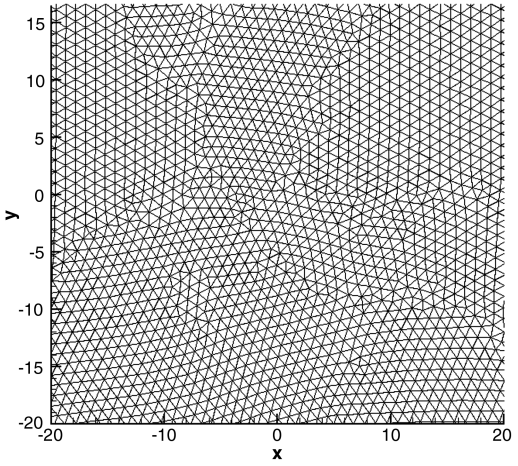

Fig. 25 Mesh topology used in the test cases along the paper.

is discretized by 201×201 nodes, the interior domain with unstructured triangles (Fig. 25). The same mesh topology will be used along the paper with the same degree of freedom as in the reference paper. The perturbation velocities, density and pressure are normalized by c_0 (ambient speed of sound), ρ_0 (ambient density) and $\rho_0 c_0^2$ respectively. Figure 26 (left-hand side) shows contour plots of density for the numerical solution at time $t = 0$ (solid lines) and $t = 30$ (dashed lines). The acoustic wave is represented by the larger circles. It is convected in the x-direction by the mean flow and propagates with the speed of sound in all directions uniformly in case of the space-time formulation, as expected. The mass-matrix discretization gives exactly the same results, therefore it is not presented. The weaker entropy wave should be just physically translated by the mean flow. A closer look to that wave reveals an important difference between the solution obtained with the mass-matrix and the space-time formulation (right plot). Indeed, a deviation from isotropy of the wave can be observed in the plot of the mass-matrix formulation (solid line). It is reported that traditional second-order methods leave an oscillatory trail [33] so the mass-matrix formulation inherits it as well. On the other hand, the truly space-time method (dashed line) does not have this unfavorable feature (despite the fact that this method is second order as well) due to the discretization along the direction of information propagation so this unsteady formulation is used for the remaining results presented in the paper.

Acoustic Sources

Any real acoustic source can be decomposed into the three basic acoustic sources: monopole, dipole, and quadrupole. Therefore, the ability to simulate wave propagation originated from these pulsating sources is a crucial requirement for LEE solvers. For validation of the discretization of these sources we use some test cases presented in the paper of Bailly and Juvé [26]. The analytical solution can be obtained via convolution of the source term and the appropriate Green function as prescribed in the aforementioned paper.

Monopole Radiation in Uniform Flow: Through this test case the P1 and P2 discretization are compared with analytical solution and with the solution obtained by finite difference method. In both cases the space-time method is used with LDA scheme. The radiation of a monopole source is investigated in subsonic and supersonic uniform mean flows. This type of source represents mass flow injection or suction in nature and is termed as thickness noise. The domain and the mesh is the same as for the benchmark problem. The monopole is implemented by using the following source vector:

$$\mathbf{S}(t, x, y) = f(x, y)\sin(\omega t)\begin{bmatrix}1\\0\\0\\1\end{bmatrix}$$

$$f(x, y) = \epsilon e^{-\alpha[(x-x_s)^2+(y-y_s)^2)]}$$

In the case of the subsonic simulation the Mach number is $M_x = 0.5$ and the source is located at the center of the domain. The following parameters identify the source: the amplitude is $\epsilon = 0.5$, the width of the source is $\alpha = \ell_n 2/2$, and the angular frequency is $\omega = 2\pi/30$. We use this test case to compare the performances of linear (P1) and quadratic elements (P2). Figure 27a shows the isocontours of pressure perturbation obtained with a quadratic discretization of the solution. In the profile we can observe two acoustic waves. The first is propagating upstream with a velocity of $1 - M$ and the wavelength is $\lambda_{\text{up}} = (1 - M)\lambda$. The second wave is propagating downstream with a velocity of $1 + M$ and the wavelength is $\lambda_{\text{down}} = (1 + M)\lambda$. On Figs. 27b and 27c we compare the solutions obtained with linear and quadratic elements on a slice done at $y = 0.0$ at $t = 270$. The reference solution of these figures is the one obtained by Bailly and Juvé [26] using a seventh-order dispersion-relation-preserving finite difference solver with a mesh having the same degree of freedom (both for P1 and P2) as the mesh used by the authors. It is difficult to see any difference between the

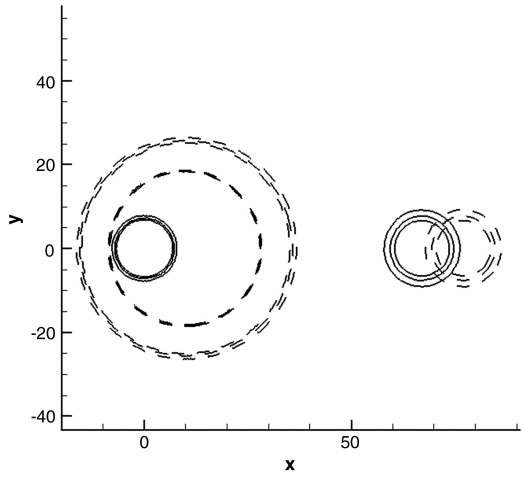

a) Density contours at initial instant (soild) and at t = 30 (dashed)

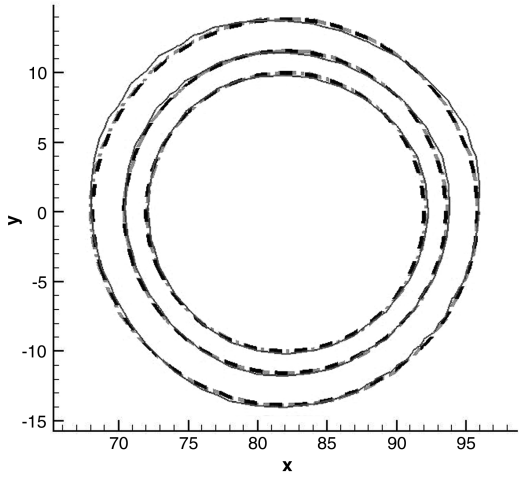

b) Zoom to the solution of the entrophy/vorticity wave at t=30 with mass-matrix (solid) and space-time formulation (dashed-dot) compared to the analytical solution (dashed)

Fig. 26 Contours of density 0.01, 0.02, 0.03.

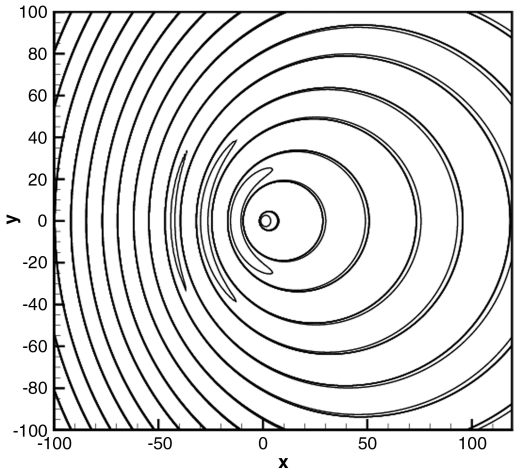

a) Pressure isocontours with values 10^{-1},10^{-2},10^{-3},10^{-4},10^{-5}

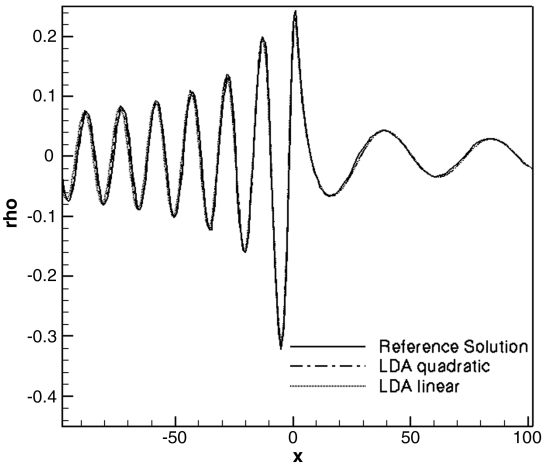

b) Pressure profile, along the axis $y = 0$

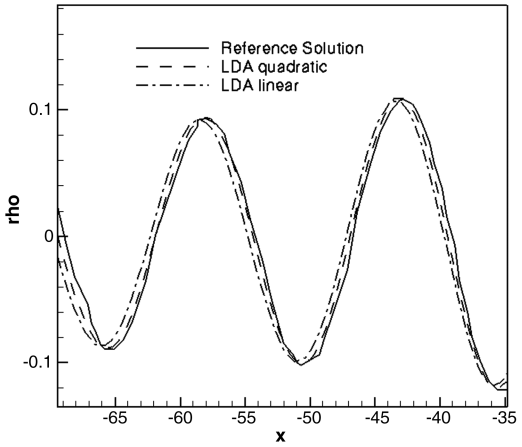

c) Zoom in on the upwind wave

Fig. 27 Monopole source in a uniform subsonic mean flow ($M = 0.5$) at $t = 270$.

two discretizations on Fig. 27b. But, when we zoom in on the upstream part like on Fig. 27c, the advantage of high-order discretization is more obvious.

The supersonic case deals with the Mach number $M = 1.5$ and the source is located at $(x_s, y_s) = (-50, 0)$. The Mach cone is defined as $M \cdot \sin(\phi)$, which gives the angle $\phi \approx 41.8°$. Now both acoustic waves propagate in the downstream direction with $M \pm 1$ and interfere with each other (Fig. 28). In the source region both the reference solution and the RDM solution fail to reproduce the analytical solution, but in different way. Bailly and Juvé [26] explain their discrepancy by the error in the calculation of the convolution in the analytical solution. However, our results follow much closer the

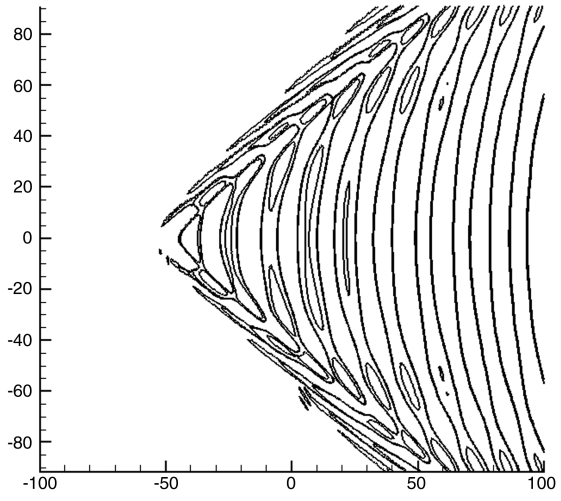

a) Pressure isocontours with values 10^{-1},10^{-2},10^{-3},10^{-4}

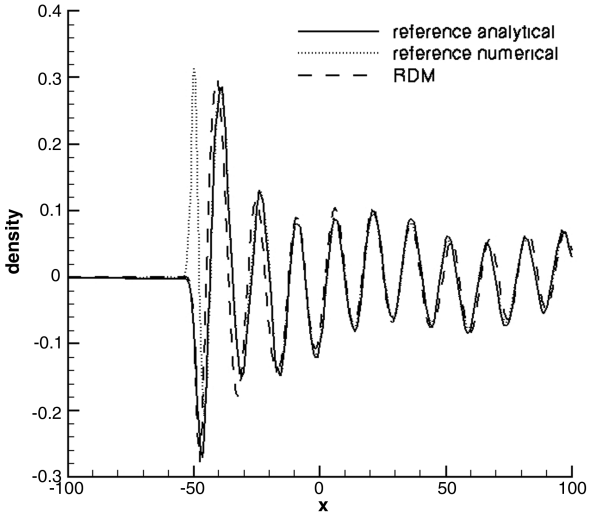

b) Pressure profile, along the axis $y = 0$

Fig. 28 Monopole source in a uniform subsonic mean flow ($M = 1.5$) at $t = 304$, compared with the data obtained by Bailly and Juvé [26].

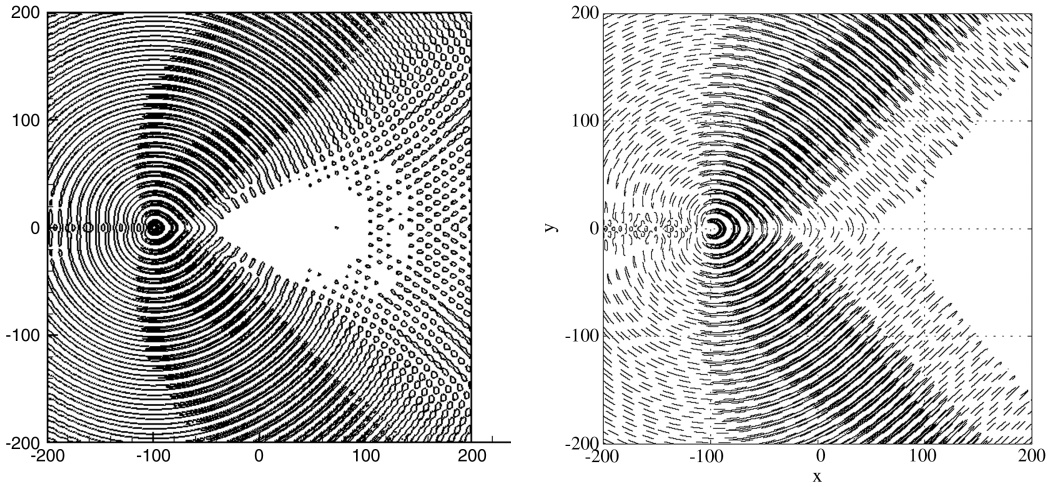

a) RDS solution

b) Solution obtained by Bailly et al. [26]
Reproduced with permission

Fig. 29 Monopole source radiation in a sheared mean flow with pressure contours from 0.001 to 0.01 (increment 0.001) and 10^{-4}.

analytical solution than the one of Bailly and Juvé. The slight discrepancy of our downwind signal is again due to the inadequate boundary treatment.

Monopole radiation in nonuniform background flow In the following, propagation in sheared mean flow will be investigated to test the ability of the system to propagate acoustic waves in inhomogeneous flowfield. Again the space-time method is used with P1 discretization. The main advantage of the LEE over the acoustic analogies is that it can handle inhomogeneous propagation domain, so reflection, refraction, and scattering effects can be taken into account. For this test case P1 discretization is considered with the same mesh as before. In the following, the monopole source is placed into a jet flow described by the Bickley's profile given as:

$$u_0 = \frac{M}{\cos h^2[(1+\sqrt{2})y/b]}$$

The axial Mach number is $M = 0.5$, the half-width of the jet is $b = 10$. The width of the source is $\alpha = \ell_n 2/9$, the amplitude $\varepsilon = 0.01$ and the center of the monopole source is $(x_s, y_s) = (-100, 0)$, which lies in the center of the jet. The angular frequency is taken to $\omega = 2\pi/9$. In this way the wavelength ($\lambda = 9$) of the source is close to the half-width of the jet causing strong refraction, so the radiation pattern is modified by the mean flow gradient as can be seen in Fig. 29. A shadow region is formed in the downstream direction near the angle given by $\phi = \frac{1}{1+M} \approx 48°$.

Conclusions

This paper shows that the RDM is an alternative method to resolve acoustic waves through LEEs. Because of the multidimensional upwind formulation, high accuracy was achieved with the basic test cases on unstructured grids. One of the main advantage of RDM is the continuous representation of flow variables resulting in less memory requirement than the discontinuous Galerkin method. It is also applicable for unstructured grids with even higher level of accuracy than for structured meshes as shown in the grid sensibility study.

Two different types of consistent time-integration approach are considered in this paper. Through analytical wave number analysis the two methods were characterized and found that the mass-matrix approach owns the same behavior as the traditional methods, i.e., as the time-step of the simulation is getting smaller, the discretization is exact for wider range of frequencies. In the case of space-time analysis, however, there exists an optimal CFL number, where the discretization provides correct phase-speed and acceptable dissipation for the widest range of wave numbers. This optimum is related to the shape of prismatic discretization of time. The best results are obtained around the element having the least aspect ratio.

It is observed as well that RDM faces the same numerical issues as the finite difference and discontinuous Galerkin methods, such as the necessity of higher-order discretization to reduce the grid dependency and more adequate nonreflecting boundary conditions.

Acknowledgment

This research is supported through the Marie Curie Research Training Network Project AETHER (contract no MRTN-CT-2006-035713) and the SBO project CAPRICORN (contract number IWT-SBO-050163).

References

[1] Tam, C. K. W., "Computational Aeroacoustics: An Overview of Computational Challenges and Applications," *International Journal of Computational Fluid Dynamics*, Vol. 18, No. 6, 2004, pp. 547–567. doi:10.1080/10618560410001673551

[2] Colonius, T., and Lele, S. K., "Computational Aeroacoustics: Progress on Nonlinear Problems of Sound Generation," *Progress in Aerospace Sciences*, Vol. 40, No. 6, 2004, pp. 345–416. doi:10.1016/j.paerosci.2004.09.001

[3] Tam, C. K. W., "Computational Aeroacoustics: Issues and Methods," *AIAA Journal*, Vol. 33, No. 10, 1995, pp. 1788–1796. doi:10.2514/3.12728

[4] Tam, C. K. W., and Webb, J. C., "Dispersion-Relation-Preserving Finite Difference Schemes for Computational Acoustics," *Journal of Computational Physics*, Vol. 107, No. 2, 1993, pp. 262–281. doi:10.1006/jcph.1993.1142

[5] Cockburn, B., and Shu, C. W., "TVB Runge–Kutta Local Projection Discontinuous Galerkin Method for Conservation Laws II: General Framework," *Mathematics of Computation*, Vol. 52, No. 186, 1989, pp. 411–435.

[6] Roe, P. L., "Fluctuations and Signals: A Framework for Numerical Evolution Problems," *Numerical Methods for Fluid Dynamics*, edited by K. W. Morton and M. J. Baines, Academic Press, New York, 1982, pp. 219–257.

[7] Roe, P., and Sidilkover, D., "Optimum Positive Linear Schemes for Advection in Two and Three Dimensions," *SIAM Journal on Numerical Analysis*, Vol. 29, No. 6, 1992, pp. 1542–1568. doi:10.1137/0729089

[8] Sidilkover, D., and Roe, P., "Unification of Some Advection Schemes in Two Dimensions," ICASE, Technical Rept. 95-10, 1995.

[9] Ricchiuto, M., Abgrall, R., and Deconinck, H., "Application of Conservative Residual Distributive Scheme to the Solution of the Shallow Water Equations on Unstructured Meshes," *Journal of Computational Physics*, Vol. 222, No. 1, 2007, pp. 287–331. doi:10.1016/j.jcp.2006.06.024

[10] Abgrall, R., "Very High Order Residual Distribution Methods," *VKI LS 2006-01 CFD: Higher Order Discretization Methods*, von Kármán

Institute for Fluid Dynamics, Rhode-St-Genèse, Belgium, 2005, pp. 1–53.

[11] Tave, C., Villedieu, N., Ricchiuto, M., Abgrall, R., and Deconinck, H., "Very High-Order Residual Distribution on Triangular Grids," *Proceedings of Eccomas CFD 2006*, edited by J. P. P. Wesseling, and E. Oñate, Egmond aan Zee, The Netherlands, Sept. 2006.

[12] Villedieu–Ligout, N., Ricchiuto, M., and Deconinck, H., "High-Order Residual Distribution Schemes: Discontinuity Capturing Crosswind Dissipation and Diffusion," *Computational Fluid Dynamics 2006: Proceedings of the Fourth International Conference on Computational Fluid Dynamics* [CD-ROM 90-9020970-0], ICCFD, Ghent, Belgium, July 2006.

[13] Abgrall, R., and Mezine, M., "Construction of Second-Order Accurate Monotone and Stable Residual Distribution Schemes for Unsteady Flow Problems," *Journal of Computational Physics*, Vol. 188, No. 1, 2003, pp. 16–55. doi:10.1016/S0021-9991(03)00084-6

[14] Csík, A., Ricchiuto, M., Deconinck, H., and Poedts, S., "Space-Time Residual Distribution Schemes for Hyperbolic Conservation Laws," *15th AIAA Computational Fluid Dynamics Conference*, AIAA No, 2001-2617, 2001.

[15] Dobeš, J., Ricchiuto, M., and Deconinck, H., "Implicit Space-Time Residual Distribution Method for Unsteady Laminar Viscous Flow," *Computers and Fluids*, Vol. 34, Nos. 4–5, 2005, pp. 617–640. doi:10.1016/j.compfluid.2003.09.006

[16] De Palma, P., Pascazio, G., Rossiello, G., and Napolitano, M., "A Second-Order Accurate Monotone Implicit Fluctuation Splitting Scheme for Unsteady Problems," *Journal of Computational Physics*, Vol. 208, No. 1, 2005, pp. 1–33. doi:10.1016/j.jcp.2004.11.023

[17] Ricchiuto, M., "Construction and Analysis of Compact Residual Discretizations for Conservation Laws on Unstructured Meshes," Ph.D. Thesis, Université Libre de Bruxelles, Brussels, Belgium, 2005.

[18] van der Weide, E., "Compressible Flow Simulation on Unstructured Grids Using Multi-Dimensional Upwind Schemes," Ph.D. Thesis, Technische Universiteit Delft, Delft, The Netherlands, 1998.

[19] Ferrante, A., and Deconinck, H., "Solution of the Unsteady Euler Equations Using Residual Distribution and Flux Corrected Transport," von Kármán Institute for Fluid Dynamics, Tech. Rept. VKI PR 1997-08, 1997.

[20] Ricchiuto, M., Csík, A., and Deconinck, H., "Residual Distribution for General Time Dependent Conservation Laws," *Journal of Computational Physics*, Vol. 209, No. 1, 2005, pp. 249–289. doi:10.1016/j.jcp.2005.03.003

[21] Ricchiuto, M., Abgrall, R., and Deconinck, H., "Construction of Very High Order Residual Distributive Schemes for Unsteady Scalar Advection: Preliminary Results," *33rd Computational Fluid Dynamics: Novel Methods for Solving Convection Dominated Systems*, Vol. 5, von Kármán Institute for Fluid Dynamics, Rhode-St-Genèse, Belgium, 2003, pp. 1–24.

[22] Villedieu, N., Koloszar, L., Quintino, T., and Deconinck, H., "Unsteady High Order Residual Distribution Schemes with Applications to Linearised Euler Equations," *Numerical Mathematics and Advanced Applications*, Springer–Verlag, New York, 2009–2010, pp. 911–919.

[23] Abgrall, R., "Towards the Ultimate Conservative Scheme: Following the Quest," *Journal of Computational Physics*, Vol. 167, No. 2, 2001, pp. 277–315. doi:10.1006/jcph.2000.6672

[24] Anthoine, J., "Unsteady Flow Modeling and Computation," *VKI LS on Basics of AeroAcoustics and Thermoacoustics*, von Kármán Institute for Fluid Dynamics, Rhode-St-Genèse, Belgium, 2007, pp.1–65.

[25] Villedieu, N., "Study of Third Order Residual Distributive Schemes for Advection-Diffusion," von Kármán Institute for Fluid Dynamics, Tech. Rept. No. VKI PR 2004-24, 2004.

[26] Bailly, C., and Juvé, D., "Numerical Solution of Acoustic Propagation Problems Linearized Euler Equations," *AIAA Journal*, Vol. 38, No. 1, 2000, pp. 22–29. doi:10.2514/2.949

[27] Koloszar, L., Villedieu, N., Quintino, T., Anthoine, J., and Rambaud, P., "Application of Residual Distribution Method for Acoustic Wave Propagation," *3rd European Conference for Aerospace Science*, EUCASS, Versailles, France, July 2009, p. 265.

[28] Thompson, K., "Time Dependent Boundary Conditions for Hyperbolic Systems," *Journal of Computational Physics*, Vol. 68, No. , 1987.

[29] Hirsch, C., *Numerical Computations of Internal and External Flows I–II*, Wiley, New York, 1990, pp. 152–153.

[30] Paillere, T., "Multidimensional Upwind Residula Distribution Schemes for the Euler and Navier–Stokes Equations on Unstructured Grids," Ph.D. Thesis, Université Libre de Bruxelles, Brussels, Belgium, June 1995.

[31] Lani, A., Quintino, T., Kimpe, D., Deconinck, H., Vandewalle, S., and Poedts, S., "The COOLFluiD Framework: Design Solutions for High-Performance Object Oriented Scientific Computing Software," *Computational Science: ICCS 2005*, Vol. 1, Springer–Verlag, New York, 2005, pp. 279–286.

[32] Quintino, T., "A Component Environment for High-Performance Scientic Computing, Design and Implementation," Ph.D. Thesis, Katoliek Universiteit Leuven, Leuven, Belgium, Dec 2008.

[33] Hardin, J. C., Ristorcelli, J. R., and Tam, C. K. W., "ICASE/LaRC Workshop on Benchmark Problems in Computational Aeroacoustics (CAA)," NASA CP 3300, 1995.

C. Bailly
Associate Editor